

1 **The Atr-Chek1 pathway inhibits axon regeneration in response to Piezo-dependent**
2 **mechanosensation**

3 Feng Li^{1,2,10}, Tsz Y. Lo^{1,10}, Leann Miles^{3,10}, Qin Wang^{1,2,10}, Dan Li¹, Jingwen Niu⁴, Jessica I
4 Goldshteyn¹, Chuxi Wang¹, Shuchao Wang¹, Jingyun Qiu¹, Shannon Trombley¹, Katarzyna
5 Pogoda^{5,6}, Megan Brewster⁷, Panteleimon Rompolas⁷, Ye He⁸, Paul A. Janmey⁵, Gareth M.
6 Thomas^{4,9}, Yuanquan Song^{1,2*}

7 ¹Raymond G. Perelman Center for Cellular and Molecular Therapeutics, The Children's Hospital
8 of Philadelphia, Philadelphia, PA 19104, USA

9 ²Department of Pathology and Laboratory Medicine, University of Pennsylvania, Philadelphia,
10 PA 19104, USA

11 ³The Graduate Group in Biochemistry and Molecular Biophysics, University
12 of Pennsylvania, Philadelphia, PA 19104, USA

13 ⁴Shriners Hospitals Pediatric Research Center (Center for Neurorehabilitation and Neural Repair),
14 Temple University School of Medicine, Philadelphia, PA 19140, USA

15 ⁵Institute for Medicine and Engineering, University of Pennsylvania, Philadelphia, PA 19104,
16 USA

17 ⁶Institute of Nuclear Physics, Polish Academy of Sciences, PL-31342, Krakow, Poland

18 ⁷Department of Dermatology, University of Pennsylvania, Philadelphia, PA 19104, USA

19 ⁸The City University of New York, Graduate Center - Advanced Science Research Center,
20 Neuroscience Initiative, New York, NY 10031, USA

21 ⁹Department of Anatomy and Cell Biology, Temple University School of Medicine, Philadelphia,
22 PA 19140, USA

23 ¹⁰These authors contributed equally to this work

24 *Correspondence: songy2@email.chop.edu

25

26 **ABSTRACT**

27 **Atr is a serine/threonine kinase, known to sense single-stranded DNA breaks and activate**
28 **the DNA damage checkpoint by phosphorylating Chek1, which inhibits Cdc25, causing cell**
29 **cycle arrest. This pathway has not been implicated in neuroregeneration. We show that in**
30 ***Drosophila* sensory neurons, removing Atr or Chek1, or overexpressing Cdc25 promotes**
31 **regeneration, whereas Atr or Chek1 overexpression, or Cdc25 knockdown impedes**
32 **regeneration. Inhibiting the Atr-associated checkpoint complex in neurons promotes**
33 **regeneration and improves synapse/behavioral recovery after CNS injury. Independent of**
34 **DNA damage, Atr responds to the mechanical stimulus elicited during regeneration, via the**
35 **mechanosensitive ion channel Piezo and its downstream NO signaling. Sensory neuron-**
36 **specific knockout of Atr in adult mice, or pharmacological inhibition of Atr-Chek1 in**
37 **mammalian neurons *in vitro* and in flies *in vivo* enhance regeneration. Our findings reveal**
38 **the Piezo-Atr-Chek1-Cdc25 axis as an evolutionarily conserved inhibitory mechanism for**
39 **regeneration, and identify potential therapeutic targets for treating nervous system**
40 **trauma.**

41

42 **INTRODUCTION**

43 Axon regeneration in the adult central nervous system (CNS) is rather limited, due to the
44 diminished regenerative potential of mature neurons and the inhibitory microenvironment¹⁻⁴. As
45 a result, permanent disability often occurs in individuals with spinal cord injury or stroke. By
46 contrast, neurons in the peripheral nervous system (PNS) are generally capable of robust axon

47 regeneration and regain functional recovery after injury. However, in cases of severe peripheral
48 nerve insults, such as proximal nerve lesions or complete transections, neurological deficits can
49 still occur due to the slow rate of spontaneous axon regeneration, failure of reinnervation or the
50 development of chronic pain⁵. In humans particularly, minimal clinically meaningful restoration
51 of motor function has been observed⁶⁻⁸. Moreover, the regenerative capacity of the PNS declines
52 with aging⁹. Therefore, strategies need to be developed to increase the rate and/or extent of axon
53 regeneration to improve functional outcomes in the adult mammalian CNS and PNS.

54 To achieve this goal, a major focus of research is to identify the neuronal intrinsic
55 molecular machinery that triggers the regenerative response or acts as a regeneration brake.
56 Various injury paradigms in different model organisms have been established¹⁰ that serve as
57 screening platforms. We previously developed a *Drosophila* peripheral sensory neuron injury
58 model that displays neuronal type-specific regeneration: class IV but not class III dendritic
59 arborization (da) sensory neurons are able to regenerate¹¹. Utilizing this tool, we have performed
60 genetic screens and identified the RNA processing enzyme *Rtca* as an evolutionarily conserved
61 inhibitor of axon regeneration, which links axon injury to ER stress and RNA modifications¹².
62 We have thus performed an additional screen on other cellular stress pathways focusing on the
63 DNA damage response (DDR). We found that mediators of the DNA single-strand break (SSB)
64 response specifically inhibit axon regeneration.

65 SSBs are known to activate *Atr* (ataxia telangiectasia and Rad3 related), a
66 serine/threonine kinase that directly phosphorylates *Chek1* (checkpoint kinase-1). *Chek1* in turn
67 phosphorylates and inhibits the phosphatase *Cdc25C* (cell division cycle 25C) or *Cdc25A*, which
68 would prevent *Cdk1*(cyclin-dependent kinase 1)/*CycB* (cyclin B) from being dephosphorylated
69 and therefore cause a cell cycle arrest in G2/M or S-phase, respectively^{13, 14}. A multistep model

70 has been proposed for Atr checkpoint activation in response to DNA damage¹⁵, which involves
71 DNA damage sensing, signal transduction and execution. DNA damage generates ssDNA
72 (single-stranded DNA), which is recognized and coated by RPA (Replication protein A). The
73 primed ssDNA recruits Atr-Atrip (Atr interacting protein) and facilitates the loading of 9-1-1
74 (Rad9-Hus1-Rad1) by the Rad17 complex. The 9-1-1 complex may then stimulate the kinase
75 activity of Atr-Atrip, leading to phosphorylation of its substrates including Rad17 and Rad9.
76 Phosphorylated Rad17 and Rad9 may facilitate the recruitment of downstream signaling proteins
77 Claspin and TopBP1 (topoisomerase (DNA) II binding protein 1), allowing them to be efficiently
78 phosphorylated by Atr. Phosphorylated TopBP1 may further stimulate the kinase activity of Atr,
79 whereas phosphorylation of Claspin may promote the phosphorylation and activation of Chek1.

80 Atr can also be activated by mechanical force. It has been reported that Atr can respond
81 to mechanical stimuli, such as osmotic stress, in mediating chromosome dynamics, which is
82 independent of DNA damage¹⁶. However, the underlying mechanoreceptor remains unknown.
83 We have recently demonstrated that the mechanosensitive (MS) ion channel Piezo is activated
84 during axon regrowth, leading to local elevation of calcium transients and the activation of the
85 Nos (nitric oxide synthase) cascade to restrict axon regrowth, and that Piezo loss of function
86 (LOF) promotes class III da neuron axon regeneration¹⁷. The downstream cellular and molecular
87 signaling of Piezo-Nos, however, remains elusive. Moreover, mammalian Piezo1 can be
88 activated by osmotic stress¹⁸ and also functions as a regeneration inhibitor¹⁷. Here we show that
89 Atr-Chek1 and the associated checkpoint complex act downstream of Piezo to suppress axon
90 regeneration by inactivating Cdc25-Cdk1. Instead of sensing DNA damage, Atr responds to the
91 mechanical stress elicited after axon injury, with Piezo as the mechanosensor and NO (nitric
92 oxide) as the mediator. We further show that blocking Atr-Chek1 promotes axon regeneration

93 both in the PNS and CNS, leading to synapse regeneration and behavioral recovery. The function
94 of Atr-Chek1 in inhibiting axon regeneration appears to be evolutionarily conserved in
95 mammals. This study identifies an unexpected role of the Atr-Chek1 kinase cascade in regulating
96 neuroregeneration, reveals a mechanistic link to the mechanosensitive ion channel Piezo, and
97 provides potential therapeutic targets for stimulating nerve repair.

98

99 **RESULTS**

100 **Atr-Chek1-Cdc25-Cdk1 regulate axon regeneration**

101 We used the previously described *Drosophila* da sensory neuron injury model^{11,12} to study axon
102 regeneration. In brief, using a two-photon laser, we injured the axon of the mechanosensitive
103 class III da neurons (labeled with *19-12-Gal4>CD4tdGFP, repo-Gal80*) in the PNS of early 3rd
104 instar larvae. Degeneration of the distal axon was confirmed at around 24 hours after injury (h
105 AI) and regeneration was assessed at around 72 h AI (Fig. 1a). In contrast to wild-type (WT)
106 class III da neurons which failed to regenerate (Fig. 1a, arrow), in a null mutant¹⁹ of the
107 *Drosophila* homologue of Atr – *meiotic 41/mei41*^{29D}, new axons regrew substantially beyond the
108 injury site (Fig. 1a, arrowheads). The function of Atr/mei41 is cell-autonomous because its RNAi
109 knockdown in class III da neurons (*19-12-Gal4>mei41 RNAiV103624*) recapitulated the
110 enhancement of regeneration. As expected, class III da neuron specific RNAi knockdown of the
111 fly homologue of Chek1 – grapes/grp (*19-12-Gal4>grp RNAiBL27277* and *19-12-Gal4>grp*
112 *RNAiV10076*), or *grp*^{A196} mutant clones of class III da neurons (using MARCM²⁰) also enhanced
113 axon regeneration, similarly to Atr/mei41 deficiency (Fig. 1a, arrowheads). On the other hand,
114 class III da neuron specific overexpression of *twine/twe* or *string/stg* (*19-12-Gal4>twe* or *19-12-*
115 *Gal4>stg*), the fly homologues of Cdc25C/Cdc25A which are negatively regulated by Chek1,

116 promoted axon regeneration (Fig. 1a, arrowheads). Cdc25 is known to activate Cdk1 by
117 removing the inhibitory phosphorylation at tyrosine 15 (Y15) and the adjacent threonine (T14)
118 residues¹⁴. We therefore overexpressed the phospho-acceptor mutant of Cdk1 –
119 Cdk1.T14A.Y15F, which renders it unable to be phosphorylated and is thus the activated form²¹,
120 in class III da neurons (*19-12-Gal4> Cdk1.T14A.Y15F*). We found that it was sufficient to
121 trigger axon regeneration (Fig. 1a, arrowheads). Moreover, knocking down Cdc25/twe in class
122 III da neurons in the *mei41^{29D}* background abolished the enhanced regeneration phenotype (Fig.
123 1a, arrow), consistent with a model in which Cdc25/twe lies downstream of Atr/mei41 to
124 regulate axon regeneration. The regeneration phenotype was further quantified by assessing the
125 “Regeneration percentage” and “Regeneration index” (Fig. 1b, c, Supplementary Fig. 1a and
126 Methods), as described previously¹¹. We also quantified class III da neuron dendrite branching
127 after blocking the Atr pathway and did not observe obvious change in total dendrite length
128 (Supplementary Fig. 1b), suggesting a specific role of this pathway in axon regeneration.

129 Conversely, we determined whether gain of function (GOF) of Atr-Chek1 would reduce
130 the regenerative potential of class IV da neurons, which are normally capable of regeneration¹¹.
131 We labeled class IV da neurons with *ppk-CD4tdGFP* and used the following injury paradigm:
132 axotomy was induced at 3rd instar, degeneration was confirmed at 24 h AI and regeneration was
133 assayed at 48 h AI¹². Compared to WT class IV da neurons, which exhibited axon regeneration
134 about 80% of the time (Fig. 1d-f, arrowheads), overexpression of wild-type human ATR (hATR-
135 WT) in class IV da neurons significantly reduced the axon regeneration percentage to 50% and
136 decreased the length of the regrown axons (Fig. 1d-f, arrows). However, its kinase dead version
137 (hATR-KD) did not significantly alter regeneration (Fig. 1d-f, arrowheads), indicating that the
138 kinase activity of Atr is required for regeneration inhibition. Consistent with this finding,

139 overexpression of Chek1/grp or human CHEK1 (hCHEK1) also led to reduced class IV da
140 neuron axon regeneration (Fig. 1d-f, arrows). The fact that human ATR and CHEK1 are both
141 capable of inhibiting axon regeneration in flies suggests that the role of Atr-Chek1 in mediating
142 regeneration may be evolutionarily conserved. This was further confirmed by analyzing their
143 role in mammalian axon regeneration (see below). Moreover, RNAi knockdown of Cdc25/twe in
144 class IV da neurons, or LOF of Cdk1^{22,23} as in transheterozygotes of *Cdk1*^{B47/E1-23} impeded axon
145 regeneration to a similar extent (Fig. 1d-f, arrows). Lastly, hATR-WT failed to inhibit axon
146 regeneration when co-expressed with the constitutively active Cdk1 (T14A, Y15F) (Fig. 1d-f),
147 confirming that Cdk1 functions downstream of Atr in regulating axon regeneration. Together,
148 these LOF and GOF analyses demonstrate that the Atr-Chek1 cascade modulates
149 neuroregeneration, with Atr/mei41-Chek1/grp and Cdc25/twe-Cdk1 functioning as anti- and pro-
150 regeneration factors, respectively.

151 We next examined the expression pattern of Atr/mei41 using a transgenic fly that
152 contains a fosmid clone of the FLAG tagged mei41 genomic locus – mei41::FLAG, so that
153 FLAG expression reflects the endogenous pattern of mei41 at the physiological level²⁴. We
154 found that mei41::FLAG is present in class III da neurons, restricted within the nucleus
155 (Supplementary Fig. 1c, red dashed circle). We did not detect obvious differences in the
156 expression level or distribution of mei41::FLAG between uninjured and injured class III da
157 neurons at 24 or 48 h AI (Supplementary Fig. 1c). The expression of mei41::FLAG was also
158 found in other types of da neurons, including class IV da neurons (Supplementary Fig. 1c, yellow
159 dashed circle), suggesting that Atr/mei41 *per se* is likely not a determining factor for the
160 regeneration cell type specificity.

161 To determine the specificity of the Atr-Chek1 pathway in regulating regeneration, we

162 queried the other classical DDR branch which is triggered by double-strand DNA breaks (DSB).
163 Once DSBs are generated, Atm (ataxia telangiectasia mutated) is recruited by the Mre11-Rad50-
164 Nbs1 (MRN) complex to sites of broken DNA and phosphorylates downstream substrates such
165 as Chek2 (checkpoint kinase 2)¹³. The fly homologues of Atm, Rad50 and Nbs are telomere
166 fusion/tefu, rad50 and nbs1, respectively. We found that their LOF mutations, as in *tefu*^{atm-6}²⁵,
167 *rad50*^{EPI}²⁶ and *nbs1*²⁷ did not result in significant defects in class IV da neuron axon
168 regeneration (Supplementary Fig. 2a, b). Furthermore, LOF of Atm/tefu as in *tefu*^{atm-6/atm-3}²⁵ did
169 not lead to enhanced axon regeneration in class III da neurons (Supplementary Fig. 2c-e, arrow).
170 These observations highlight the unique role of the Atr-Chek1 pathway in mediating
171 neuroregeneration and also raise the question whether DNA damage is indeed involved.
172 Moreover, we examined the axon regeneration phenotype in the regeneration-incompetent class I
173 da neurons¹¹ and found that *Atr/mei41* mutants also showed increased regeneration
174 (Supplementary Fig. 2f-h, arrowheads). This suggests that the regeneration-inhibition function of
175 the Atr pathway is applicable to multiple neuronal cell types, as is further exemplified by our
176 regeneration studies in mammals (see below).

177

178 **Atr-Chek1 inhibits axon regeneration independent of DNA damage**

179 In the DDR, ssDNAs induced by DNA damage are sensed by RPAs, which then recruit and
180 activate Atr, orchestrated by additional factors. The imminent question is whether DNA damage
181 is implicated in Atr activation during neuroregeneration. To address this question, we first
182 assessed whether DNA damage is induced after axon injury in class III da neurons. γ H2AX
183 (H2A histone family, member X) – the serine 139 phosphorylated form of H2AX serves as the
184 gold standard DNA damage marker^{28, 29}. Its fly homologue is His2Av and a phospho-specific

185 antibody against His2Av – p-His2Av has been widely used for detecting DNA damage in flies³⁰.
186 Using this antibody, we found there was no difference, in terms of p-His2Av staining, between
187 injured and uninjured class III da neurons at 5 min, 24 h or 48 h AI (Fig. 2a, dashed circles),
188 suggesting that DNA damage is not significantly induced after axon injury or during axon
189 regeneration in da sensory neurons. Second, we tested whether His2Av LOF affects axon
190 regeneration and found that class III da neuron specific knockdown of His2Av with a previously
191 reported RNAi³¹ did not increase axon regeneration (Fig. 2b-d, arrow). Third, we asked whether
192 blocking the ssDNA sensing step by eliminating RPAs would interfere with Atr's function in
193 regeneration. RPA is a heterotrimer composed of three subunits Rpa1, Rpa2 and Rpa3.
194 Therefore, we expressed in class III da neurons RNAis targeting their fly homologues RpA-70,
195 RPA2 and RPA3 and found no enhancement of axon regeneration (Fig. 2b-d, arrow). This was
196 further confirmed by the *RPA2*^{KG00759} amorphic mutant³² class III da neurons (using MARCM)
197 and the *RPA3*^{G0241} LOF allele³³ (Fig. 2b-d, arrow). Lastly, overexpression of RpA-70, RPA2 or
198 RPA3 in class IV da neurons did not reduce their axon regeneration (Supplementary Fig. 3a, b).
199 These data strongly suggest that the neuronal intrinsic DDR does not contribute significantly to
200 injury-induced axon regeneration in da sensory neurons, and that the Atr-Chek1 pathway inhibits
201 axon regeneration independent of DNA damage.

202

203 **The Atr-associated checkpoint complex inhibits axon regeneration**

204 The RPA-mediated DNA damage sensing step is thus dispensable for Atr's inhibition of axon
205 regeneration. However, we wondered whether other factors in the checkpoint complex, which
206 are important for the signal transduction and execution steps, facilitate the regulation of
207 regeneration. We focused on Atrip, Rad17, the 9-1-1 complex composed of Rad9-Hus1-Rad1,

208 TopBP1 and Claspin (Fig. 3b). We found that class III da neuron specific RNAi knockdown
209 targeting their fly homologues *Atrip/mus304*, *Rad17*, *Rad1*, *TopBP1/mus101* and *Claspin* all
210 markedly increased axon regeneration (Fig. 3a, c, d, arrowheads). The regeneration enhancement
211 phenotype via *TopBP1/mus101* RNAi knockdown was recapitulated in a LOF mutation –
212 *mus101^A* (Fig. 3a, c, d, arrowheads). Moreover, LOF of *Hus1-like*, the fly homologue of *Hus1*,
213 in an insertional allele *Hus1-like^{M11259}* which abolished its expression (Supplementary Fig. 4b,
214 c), also promoted axon regeneration (Fig. 3a, c, d, arrowheads). Because the *Hus1-like* insertion
215 was also mapped to the promoter region of a neighboring gene – *ctrip* (Supplementary Fig. 4a),
216 we thus analyzed an insertional mutant of *ctrip* – *ctrip^{M114762}*, but did not observe a regeneration
217 phenotype in class III da neurons (Supplementary Fig. 4d). These data indicate that the
218 checkpoint complex known to be required for transducing the DNA damage signal is also
219 essential for facilitating Atr-Chek1 to cell autonomously inhibit neuroregeneration.

220 In order to further assess the involvement of the Atr-Chek1 pathway members in sensory
221 neuron regeneration, we determined the expression pattern of the relevant molecules we
222 analyzed in *Drosophila* and mammals. First, we examined expression of *Cdc25/twe* in da
223 neurons with antibody³⁴ staining and found it was present in both uninjured and injured class III
224 da neurons, similar to *Atr/mei41* (Supplementary Fig. 5a). Second, we performed
225 immunostaining for *Atrip*, *Chek1* and *TopBP1* using mouse dorsal root ganglion (DRG) tissues,
226 and found that each of these proteins was expressed with/without sciatic nerve lesion (SNL)
227 (Supplementary Fig. 5b). Third, as extensive gene expression analyses had been performed in
228 mouse and human DRGs, we thus queried the transcript level of Atr-Chek1 pathway members in
229 a number of these databases^{35,36}, and found that they were all expressed in the mouse or human
230 DRG, although at a low to medium level (Supplementary Fig. 5c). This is consistent with a

231 potential homeostatic function of this pathway in non-dividing cells.

232

233 **Blocking the Atr-Chek1 pathway promotes behavioral recovery and synapse regeneration**

234 Initiation of axonal regrowth is only the first step towards repairing lost connections. True repair

235 requires that regenerating axons find their targets and reform functional synapses. In general, this

236 process of functional regeneration is poorly studied in the field. To our knowledge, this has never

237 been documented in any *Drosophila* injury models³⁷. To assess functional recovery in flies, we

238 utilized a behavioral paradigm based on the larval gentle-touch response³⁸ – gently touching

239 larval anterior segments (thoracic (T) segments and the first abdominal segment) with an eyelash

240 elicits a set of stereotypical responses that are readily quantifiable (Supplementary Fig. 6b). We

241 further subcategorized the intensity of the gentle-touch stimulus based on the contact area

242 between the eyelash and the body segment: touch+, touch++ and touch+++, with the eyelash

243 diameter covering $<1/8$, $1/8-1/4$ or $1/4-1/2$ of the segment, respectively (Supplementary Fig. 6a).

244 Larvae showed a graded response according to the stimulation intensity (Fig. 4c, e, g and

245 Supplementary Fig. 6d-f). As shown previously, the mechanosensitive class III da neurons

246 mediate gentle-touch sensation³⁹. We further found that there is a segment-wise somatosensory

247 map for gentle-touch: class III da neuron axons project into the VNC (ventral nerve cord) in an

248 anterior-posterior pattern, that is, axons from the T1 segment constitute the anterior-most T1

249 bundle within the VNC (Fig. 4a), and that injuring the class III da neuron axon bundle at T1 or

250 T2 in the VNC (Fig. 4a) led to an impaired touch response specifically at segment T1 or T2,

251 without affecting neighboring segments (Supplementary Fig. 6c).

252 Given this precision, we injured class III da neuron axons at the T1 & T2 bundles in the

253 VNC, then specifically stimulated the T1, T2, T3 or A1 (abdominal) segment, and scored the

254 touch response at 8, 24 and 48 h AI. We found that in WT control, axon injury in the VNC
255 resulted in failed gentle-touch response at the T1 & T2 segments without affecting the T3 & A1
256 segments, when tested at 8 h AI (Fig. 4c, e, g and Supplementary Fig. 6d-f, Supplementary
257 Video 1). This defect persisted at 48 h AI (Fig. 4c, e, g and Supplementary Video 2), with 0%
258 and 7.3% of the larvae displayed behavioral recovery at 24 and 48 h AI (Fig. 4b, d, f and
259 Methods), respectively. We went on to assess the behavioral outcome after inhibiting the Atr-
260 Chek1 pathway focusing on *mei41*, *Rad17* and *mus101*, all of which showed strong axon
261 regeneration phenotype. Strikingly, after knocking down *Rad17* in class III da neurons, in
262 *mei41^{29D}* mutants and in particular in the *mus101* mutant – *mus101^A*, we observed substantial
263 behavioral recovery as early as 24 h AI (26%), which continued to improve at 48 h AI (43.5%)
264 (Fig. 4b, d, f and Supplementary Videos 3-6). The response score was also statistically improved
265 with the touch+++ stimulation (Fig. 4c, e, g). In the meantime, the behavioral response in the
266 uninjured T3 and A1 segments were comparable among the different genotypes (Supplementary
267 Fig. 6d-f). These results demonstrate that inhibiting the Atr-Chek1 pathway is not only beneficial
268 for axon regrowth, but also promotes functional regeneration.

269 In order to assess synapse regeneration, we first sought to confirm that class III da
270 neurons form cholinergic synapses in the CNS. We found that class III da neurons were co-
271 labeled by *nompC-QF>mCD8GFP* (the class III da neuron marker) and *ChAT-*
272 *Gal4>CD4TdTomato* (Supplementary Fig. 6g), which marks essentially all cholinergic
273 neurons⁴⁰. We used synaptotagmin-GFP (*syt.eGFP/syt*)⁴¹ to mark class III da neuron presynapses
274 (Fig. 5b), which were tightly opposed by postsynaptic cholinergic receptors labeled by α -
275 bungarotoxin (α -BTX)⁴² (Fig. 5a). We then ablated the class III da neuron axon bundles on one
276 side of the VNC, which retracted out of the neuropil within 8 h AI (Fig. 5c). At 24 h AI, WT

277 axons rarely regrew into the neuropil, displaying retraction bulb like structures (Fig. 5c). We
278 subsequently focused on the *mus101^A* mutants, as they demonstrated most robust behavioral
279 recovery. In contrast to WT, *mus101^A* mutant class III da neurons not only exhibited extensive
280 axon regeneration (~50%) back into the neuropil, but also increased the percent of regenerating
281 axons containing syt puncta, indicative of synapse reformation (Fig. 5c, d, arrowheads).

282

283 **Atr functions downstream of Piezo and Nos in regulating axon regeneration**

284 Since Atr is not activated by DNA damage during neuroregeneration, what, then, is the trigger?
285 We speculated that mechanical stimulus may be the culprit, based on several lines of evidence.
286 First, mechanical stress such as osmotic stress is capable of relocating and activating Atr, which
287 then phosphorylates Chek1¹⁶. Second, during axon regeneration, mechanical force is reported to
288 stimulate the MS ion channel Piezo, leading to local calcium elevation in the growth cone and a
289 signaling cascade mediated by Nos to inhibit regeneration¹⁷. Third, removal of Piezo or Nos
290 promotes class III da neuron axon regeneration to a similar extent as *Atr/mei41* LOF. Fourth, we
291 found that *PiezoKO* also increased class I da neuron axon regeneration as well as *Atr/mei41*
292 mutants (Supplementary Fig. 2f-h, arrowheads). Lastly, Piezo can be activated by osmotic
293 stress¹⁸. Therefore, we hypothesized that Piezo transduces the mechanical signal elicited during
294 neuroregeneration, to trigger activation of the Atr-Chek1 pathway.

295 As a first step to testing this hypothesis, we sought to determine whether Atr's response
296 to osmotic stress is Piezo-dependent. We first reproduced the hypotonic stress-induced Atr
297 relocalization/clustering phenomenon previously shown in HeLa cells¹⁶. Using WT HEK 293T
298 cells, we found that exogenously expressed FLAG tagged human ATR also formed clusters in
299 the nucleoli under hypotonic condition (Fig. 6a, dashed circles). However, in *PIEZO1* knockout

300 HEK 293T cells (*PIEZO1KO*)⁴³, ATR clusters were much less abundant. Even if they were
301 induced, they appeared smaller in size and showed reduced fluorescence intensity (Fig. 6a-c).
302 We then went on to determine whether Atr clustering relies on Nos, as it is downstream of Piezo.
303 We pharmacologically manipulated NOS, and found that inhibiting NOS with 1400W
304 dihydrochloride⁴⁴ attenuated the ATR clustering induced by hypotonic stress, whereas activating
305 NOS with histamine⁴⁵ rescued the reduced ATR clustering in *PIEZO1KO* (Fig. 6d-f). These
306 results indicate that the mechanical stress-induced Atr relocalization relies on the presence of
307 Piezo and Nos, and that Piezo can function as a mechanoreceptor underlying Atr's response to
308 mechanical stimulus.

309 Second, we performed genetic interaction and epistasis analyses to determine the
310 relationship between Atr/mei41 and the Piezo-Nos pathway. Genetic interaction analyses showed
311 that while transheterozygotes of *mei41*^{29D/+}; *PiezoKO/+* did not show a regeneration phenotype,
312 *mei41*^{29D/+}; *Nos*^{Δ15/+} significantly promoted class III da neuron axon regeneration, similar to
313 homozygous mutants of *mei41*^{29D}, *PiezoKO* or *Nos*^{Δ15} (Fig. 7a-c). This result indicates that
314 Atr/mei41 and Piezo-Nos function in the same genetic pathway, and further suggests that,
315 although Atr/mei41 does not associate with Piezo *per se*, it appears to closely interact with Nos.
316 Moreover, our epistasis analysis showed that: 1) class III da neuron-specific overexpression of
317 Chek1/grp reduced the enhanced regeneration phenotype in *PiezoKO*; 2) overexpression of
318 Chek1/grp also attenuated the regeneration enhancement in *Nos*^{Δ15} mutants; 3) on the other hand,
319 class III da neuron specific overexpression of mPiezo1-TriM, an over-activating mutant of
320 mouse Piezo1 that reduces axon regeneration when overexpressed in class IV da neurons¹⁷, did
321 not significantly reduce the enhanced regeneration in *mei41*^{29D} mutants; 4) overexpression of
322 Nos, which inhibits axon regeneration in class IV da neurons¹⁷, also failed to attenuate the

323 regeneration phenotype in *mei41^{29D}* mutants (Fig. 7a-c). These data collectively suggest that
324 Atr/mei41 operates downstream of Piezo-Nos and that Atr/mei41 overrides the regeneration
325 phenotype that results from removal of Piezo or Nos.

326 Third, our results that Atr/mei41 genetically interacts with Nos and that Nos activity is
327 required for the mechanical stress-induced Atr clustering suggest that Piezo feeds into the Atr-
328 Chek1 pathway through NO (nitric oxide) signaling, which would be consistent with a previous
329 finding that NO promotes p53 nuclear retention in an Atr-dependent manner⁴⁶. To directly
330 visualize NO propagation, we performed NO imaging using the fluorescent NO dye DAF-FM
331 diacetate^{47,48}. While NO production was rarely detected in uninjured class III da neurons (Fig. 7f
332 and Supplementary Fig. 7), we observed obvious fluorescence signal around the axon tip, along
333 the axon and in the cell body, in 62.5% of the WT class III da neurons at 24 and 48 h AI (Fig. 7d,
334 f). As a negative control, we found that the signal of the NO dye was drastically reduced in the
335 Nos mutant – *Nos^{Δ15}* (Fig. 7d, f, g). Importantly, NO production was similarly abolished in
336 *PiezoKO* (Fig. 7e-g). This result, together with the genetic analyses, suggests that NO functions
337 as a key messenger that links the activation of the Piezo channel during axon regeneration, to the
338 downstream Atr-Chek1 pathway.

339

340 **Pharmacological and genetic inhibition of the Atr-Chek1 pathway promotes axon** 341 **regeneration in mammalian neurons *in vitro* and *in vivo***

342 Having established that hATR and hCHEK1 inhibit axon regeneration in flies, we hypothesized
343 that Atr-Chek1 may also function as regeneration inhibitors in mammals. First, we tested this
344 hypothesis using an injury paradigm in cultured neurons *in vitro* based on a microfluidic device⁴⁹,
345 ⁵⁰. In brief, embryonic (E18) rat DRG neurons were cultured in a microfluidic chamber that

346 separates the neurites from the soma. The neurites in the terminal chamber were removed by
347 vacuum aspiration at 7 days *in vitro* (DIV7) and regeneration was assessed at various time points
348 after injury. We tested the efficacy of Atr and Chek1 inhibitors in promoting axon regeneration.
349 The Atr-Chek1 network is a key mediator of DDR, and inhibiting DDR has become an attractive
350 concept in cancer therapy. To date, pharmacological inhibitors for Atr and Chek1 have already
351 entered anti-cancer clinical trials either as stand-alone agents or combined with radio- or
352 chemotherapy^{51, 52}. We thus tested two pharmacological inhibitors of Atr – AZD6738 and VE-
353 822 (NCT02157792, NCT02223923 and NCT02264678) and the Chek1 inhibitor MK-8776^{53, 54}
354 (NCT01870596). We found that inhibiting Atr with AZD6738 or VE-822, or inhibiting Chek1
355 with MK-8776 all modestly promoted axon regeneration at 18 h AI (Fig. 8a). Regrown neurite
356 coverage areas (Methods) were modestly but significantly increased in drug-treated neurons, as
357 compared to the vehicle-treated controls (Fig. 8b). The AZD6738-dependent neurite regrowth
358 enhancement was already apparent at 5 h AI (Fig 8c). We next asked whether Chek1 inhibition
359 might promote regeneration *in vivo*. To address this question, we injected the Chek1 inhibitor
360 MK-8776 directly into fly larvae immediately after axonal injury and found that this compound
361 significantly increased class III da neuron axon regeneration (Fig. 8d-f, arrowheads), compared
362 to the vehicle control (Fig. 8d-f, arrow).

363 Third, to analyze axon regeneration in mammals *in vivo*, we utilized the sciatic nerve
364 lesion (SNL) model in adult mice. To generate sensory neuron-specific Atr conditional knockout
365 (*Atr cKO*), we bred mice with *Advillin-CreER*; *Atr^{fl/fl}* alleles and induced Cre mediated
366 recombination with tamoxifen (TAM) injection (Methods). Regenerating sensory axons were
367 identified by SCG10 immunostaining⁵⁵ (Fig. 8g). We found that the extension of SCG10⁺ axons
368 was significantly increased (~60%) in *Atr cKO* compared to control animals at SNL Day 3 (Fig.

369 8g, h). To summarize, these results suggest that the Atr-Chek1 pathway also functions
370 intrinsically in neurons to inhibit axon regeneration in mammals, a process that may be
371 evolutionarily conserved, and that the anti-cancer drugs targeting Atr-Chek1 may be repurposed
372 for treating neural injury.

373

374 **Piezo exerts greater inhibition of axon regeneration on soft versus stiff substrates**

375 To begin to understand how Piezo gets activated during axon regeneration, we determined how
376 substrate stiffness affects axon growth/regrowth in the presence or absence of Piezo1, to get an
377 estimate of the range of force leading to Piezo1 activation. Specifically, we investigated whether
378 the presence of Piezo1 influences how DRG neurons respond to their environment by analyzing
379 neuronal total neurite length on the respective gel substrate that they were cultured on. To
380 generate sensory neuron specific Piezo1 conditional knockout (*Piezo1 cKO*), we bred mice with
381 *Advillin-CreER; Piezo1^{fl/fl}* alleles and induced Cre mediated recombination with TAM injection
382 (Methods). Adult DRG neurons were dissociated and cultured onto polyacrylamide (PAA)
383 hydrogels of 1.0 and 30.0 kPa (1,000 and 30,000 Pa) stiffnesses^{56, 57} for 38-40 hours. These
384 stiffnesses were chosen because DRG neurons were previously reported to exhibit increased
385 traction force at intermediate (1 kPa) to high (5 kPa) stiffnesses⁵⁸. Meanwhile, the “extreme”
386 stiffness (30.0 kPa), we hypothesized, would likely negate Piezo-mediated difference in traction
387 force, since DRG neurons produce no more than an average of 50 Pa stress⁵⁸, and the fluctuation
388 of stress that occur during extension are no more than a factor of 2 or 3⁵⁹. Indeed, we found that
389 there was no difference in total neurite growth between control and *Piezo1 cKO* groups when
390 grown on 30 kPa hydrogels (Fig. 8i, j). However, on 1.0 kPa hydrogels, *Piezo1 cKO* DRG
391 neurons exhibited significantly more total neurite length than control neurons (Fig. 8i, j),

392 suggesting that Piezo1 is likely to be activated on softer substrates. Worth mentioning, the elastic
393 modulus, a measure of the tissue's resistance to deformation, ranges from 50 to 500 Pa for
394 uninjured cortical tissues in rat, and it is even lower in injured tissues⁶⁰. Therefore, it is possible
395 that during axon regeneration, the local force between the axon tip and the environment falls into
396 the range for Piezo activation. Given its enrichment at the axon tip after injury¹⁷, these findings
397 suggest that Piezo is thus capable of transducing the physical signals to the intracellular signaling
398 cascades to slow down axon regeneration.

399

400 **DISCUSSION**

401 Mature neurons retain limited capacity to repair their injured nerve fibers after trauma, leading to
402 poor functional recovery. To overcome this regeneration failure, numerous efforts have been
403 made to increase intrinsic axon regrowth and/or remove extrinsic obstacles¹⁻⁴. However, we still
404 have limited understanding regarding how injured neurons integrate extrinsic information with
405 the intrinsic signaling pathways, to make the decision to regenerate, stall, retract or die. In this
406 study, using a *Drosophila* sensory neuron injury model, we identified the Atr-Chek1 pathway as
407 a neuron-intrinsic negative regulator of axon regeneration. We hypothesize that during axon
408 regeneration, the growth cone physically interacts with the environment such as the glial cells,
409 resulting in the activation of the mechanosensitive ion channel Piezo at the growth cone tip;
410 opening of the Piezo channels leads to local calcium influx and the activation of Nos, which then
411 produces NO; NO functions as a second messenger and propagates to the nucleus where it
412 activates Atr and its associated complex; Atr then phosphorylates and activates Chek1, which
413 phosphorylates and inactivates Cdc25, inhibiting its ability to dephosphorylate and activate Cdk1;
414 the phosphorylated and inactive Cdk1 impinges on downstream effectors, causing regeneration

415 failure (Supplementary Fig. 8).

416 The Piezo-Nos-Atr cascade thus behaves as a regeneration brake in neurons, which is
417 capable of sensing the extrinsic cues in the local microenvironment, processes and transduces
418 these signals to a kinase circuit originally known to respond to DNA damage, and then
419 potentially rewires the circuit to instruct cellular events such as cytoskeleton reorganizations to
420 curtail regeneration. Further downstream, we speculate that Cdk1 may phosphorylate multiple
421 substrates and thus engage multiple pathways. For example, Cdk1 activates FOXO⁶¹, and
422 Daf16/FOXO is inhibited by the insulin/IGF1 receptor DAF-2 during age-dependent decline of
423 axon regeneration in *C. elegans*⁶². Cdk1 also phosphorylates Ndel⁶³, which regulates dynein-
424 dependent transport, another process that is important for axon regeneration⁶⁴, associating with
425 the regulation of the cytoskeleton. Cytoskeleton dynamics, in particular microtubule and actin,
426 have been well documented as key players in axon regeneration⁶⁵. The Piezo-Nos-Atr machinery
427 is not restricted to the regeneration-incompetent class III da sensory neurons in flies, as was
428 confirmed by the presence of Atr/mei41 in other types of da neurons, and by the enhanced axon
429 regeneration of class I da neurons in *PiezoKO* or *Atr/mei41* mutants, mammalian DRG neurons
430 after pharmacological inhibition of Atr or Chek1, or in *Atr cKO*. We propose that this may be a
431 mechanism adopted by injured neurons in general, as a wait-and-see strategy, allowing them the
432 opportunity to sample the environment, assess the intrinsic status and decide whether to
433 regenerate. Furthermore, there may be a tug-of-war in all neuronal types after injury, between
434 factors that inhibit regeneration such as Piezo-Nos-Atr, and those that promote regeneration. In
435 class III da neurons, because of their limited intrinsic regenerative potential, the activation of
436 Piezo-Nos-Atr is sufficient to suppress further regeneration. However, in class IV da neurons, the
437 endogenous regenerative drive is high enough to override this blockade. The regeneration

438 enhancement phenotype observed in *Atr/mei41* mutants is comparable to that of *PiezoKO* in flies,
439 and both Piezo and Atr are shown to not only inhibit axon regeneration in fly larvae but also in
440 adult sensory neurons in mice¹⁷. These findings raise the possibility that the Atr pathway plays
441 an evolutionarily conserved role in regulating regeneration, which warrants further investigation.

442 The involvement of DNA damage in neural injury and regeneration is an emerging
443 concept, but not well explored. p53 was reported to be required for facial nerve regeneration in
444 mouse⁶⁶. Whereas inhibition of Poly (ADP-ribose) polymerases (PARPs), which are involved in
445 DNA repair, promotes axon regeneration in worms⁶⁷, no positive effect was observed in mouse⁶⁸.
446 An outstanding question is whether and how axon injury induces DDR. If it does, what type of
447 DNA damage is involved? Our results, on the other hand, favor the hypothesis that DNA damage
448 may not play a prominent role at least in fly sensory neurons after injury. However, it is worth
449 noting that we are not able to fully rule out the involvement of DNA damage, given our lack of
450 ability to specifically detect single-stranded DNA breaks in injured neurons. Moreover, NO itself
451 has been reported to act as a mutagen⁶⁹. Thus, future studies are warranted to determine the link
452 between NO and the Atr complex, and to assess additional NO targets. Another intriguing
453 question is whether other cell types in the microenvironment, for example the glial cells, undergo
454 injury-induced DDR, and if so, how that may affect the regeneration outcome.

455 Activation of the Atr kinase is well known as the initial response to DNA damage. But
456 interestingly, the Atr-Chek1 pathway is also involved in DNA-damage-independent functions.
457 Mechanical stress activates Atr at the nuclear envelope to modulate chromatin dynamics and
458 nuclear envelope plasticity¹⁶. Functions of the cytoplasmic Atr are associated with the
459 centrosome, mitochondria and cytoskeleton⁷⁰. In addition, patients with Seckel syndrome due to
460 ATR mutations, suffer severe nervous system malfunctions including microcephaly, defective

461 neurodevelopment and mental retardation⁷¹, emphasizing a crucial neural function of Atr. Our
462 work identified the missing mechanoreceptor underlying Atr's response to mechanical stimuli,
463 which is the mechanosensitive ion channel Piezo. Together with previous work demonstrating
464 Piezo's inhibitory role during axon regeneration, we have uncovered a route through which the
465 mechanical force at the growth cone is sensed, encoded, and transduced to the nucleus, to elicit a
466 signaling cascade governing cellular events such as regeneration.

467 While researchers have successfully regenerated mammalian nerves by targeting intrinsic
468 or extrinsic barriers, these exciting advancements have not yet produced successful therapeutic
469 targets for human patients. This is partly due to our incomplete understanding about the
470 pathways controlling regeneration. Another contributing factor is our limited capabilities to
471 induce proper axon regeneration beyond simply promoting axon regrowth, in order to achieve
472 adequate synapse regeneration and functional recovery. We have thus established a behavioral
473 paradigm in flies, based on the touch sensation, for assessing functional regeneration after CNS
474 injury. It is encouraging to find that inhibiting the Atr-Chek1 pathway presented beneficial
475 effects towards synapse regeneration and functional recovery. It is important to point out that the
476 enhanced behavioral recovery we observed may directly result from the *bona fide* regeneration
477 of the injured axons, although it is possible that the sprouting of uninjured axons or circuit level
478 plasticity may also contribute. Importantly, though, the fly sensory neuron injury model offers an
479 ideal opportunity to screen for novel regeneration regulators, dissect the underlying genetic,
480 cellular and molecular mechanisms, and test their functional relevance.

481 Finally, our results showing that pharmacological inhibition of Atr or Chek1 enhanced
482 axon regeneration in cultured mammalian neurons and in flies *in vivo* provide a strong rationale
483 to further test the viability of this pathway as a potential target for treating neural injury.

484 Importantly, the fact that these pharmacological inhibitors for Atr and Chek1, which are already
485 in clinical trials for cancer therapy, showed efficacy in promoting axon regeneration raises the
486 possibility of repurposing these drugs for regeneration therapy. It is worth mentioning that the
487 inhibitor induced axon regeneration *in vitro* we observed was modest, which may be due, in part,
488 to the simplified environment in the culture dish. In the absence of non-neuronal cell types such
489 as glial cells, which the growth cones interact with, the mechanical force induced suppression of
490 regeneration is less prominent compared to *in vivo*.

491

492 **FIGURE LEGENDS**

493 **Figure 1. The Atr/mei41-Chek1/grp pathway regulates axon regeneration in da sensory**
494 **neurons in flies.**

495 **(a)** Class III da neuron axons fail to regenerate in WT. Atr/mei41 removal as in *mei41*^{29D} mutants
496 or class III da neuron specific RNAi leads to increased axon regeneration. *Chek1/grp*^{A196} mutant
497 clones (with MARCM), class III da neuron expression of Chek1/grp RNAis, Cdc25/twe/stg, or
498 the dephosphorylated/activated Cdk1.T14A.Y15F increases axon regeneration. Class III da
499 neuron expression of twe RNAi suppressed the enhanced regeneration in *mei41*^{29D} mutants. The
500 injury site is demarcated by the dashed circle. Arrow marks axon stalling while arrowheads show
501 the regrowing axon tips. **(b, c)** Quantifications of class III da neuron axon regeneration with
502 Regeneration percentage (b) and Regeneration index (c). *N* = 72, 23, 30, 16, 22, 30, 36, 30, 37
503 and 28 neurons from 6 to 20 larvae. **(d)** Class IV da neurons robustly regenerate in WT. Class IV
504 da neuron specific expression of hATR-WT, grp, hCHEK1, twe RNAis, or LOF of Cdk1 as in
505 transheterozygotes of *Cdk1*^{B47/E1-23} impedes axon regeneration, whereas the kinase dead (KD)
506 mutant of hATR fails to show significant effect. Overexpression of hATR-WT together with the

507 constitutively active Cdk1 (T14A, Y15F) fails to inhibit axon regeneration. (e, f) Quantifications
508 of class IV da neuron axon regeneration. $N = 97, 50, 25, 30, 38, 33, 28, 24$ and 23 neurons from
509 6 to 18 larvae. $*P < 0.05$, $**P < 0.01$, $***P < 0.001$ by Fisher's exact test (b and e), one-way
510 ANOVA followed by Holm-Sidak's test (c) or Dunn's test (f). Scale bar = 20 μm . See also
511 Supplementary Fig. 1.

512

513 **Figure 2. The Atr-Chek1 pathway regulates axon regeneration independent of DNA**
514 **damage.**

515 (a) The DNA damage marker, phosphorylated histone 2A gamma (p-His2Av), is not upregulated
516 in injured class III da neurons at various time points, compared to the uninjured control. The
517 dashed teal circle marks the injury site and the cell bodies are outlined with dashed white lines.
518 The obvious staining in the neighboring epithelial cell nuclei serves as the positive control for
519 the antibody. (b) Class III da neuron specific expression of RNAs for His2Av, RpA-70, RPA2
520 or RPA3, $RPA2^{KG00759}$ mutant clones (with MARCM) or $RPA3^{G0241}$ mutants do not significantly
521 increase axon regeneration. (c, d) Quantifications of class III da neuron axon regeneration with
522 Regeneration percentage (c) and Regeneration index (d). $N = 72, 14, 15, 24, 16, 20, 25, 24, 24$
523 and 20 neurons from 4 to 20 larvae. The injury site is demarcated by the dashed circle. Arrow
524 marks axon stalling. No statistical difference is detected by Fisher's exact test (b), one-way
525 ANOVA followed by Holm-Sidak's test (d). Scale bar = 20 μm . See also Supplementary Fig. 2
526 and 3.

527

528 **Figure 3. The Atr-associated checkpoint complex inhibits axon regeneration.**

529 (a) TopBP1/mus101 and Hus1-like mutants, $mus101^A$ and $Hus1-like^{M11259}$, and class III da

530 neuron specific expression of Atrip/mus304 RNAs, Rad17 RNAs, Rad1 RNAs,
531 TopBP1/mus101 RNAi or Claspin RNAs increase axon regeneration. The injury site is
532 demarcated by the dashed circle. Arrow marks axon stalling while arrowheads show the
533 regrowing axon tips. **(b)** The single-stranded DNA damage pathway mediated by Atr, Chk1,
534 Cdc25 and the associated checkpoint complex. The factors marked by the red cross are tested for
535 their potential role in axon regeneration. **(c, d)** Quantifications of class III da neuron axon
536 regeneration with Regeneration percentage (c) and Regeneration index (d). $N = 72, 20, 27, 24,$
537 $30, 32, 29, 24, 23, 44, 29, 23$ and 37 neurons from 6 to 20 larvae. $*P < 0.05, **P < 0.01, ***P <$
538 0.001 by Fisher's exact test (c), one-way ANOVA followed by Dunn's test (d), two-tailed
539 unpaired Student's t-test (d). Scale bar = 20 μm . See also Supplementary Fig. 4 and 5.

540

541 **Figure 4. Inhibiting components of the Atr-associated checkpoint complex promotes**
542 **behavioral recovery after CNS injury in flies.**

543 **(a)** Class III da neuron axon projection map in the VNC and the VNC injury paradigm. There is
544 a segment-wise somatosensory map for gentle-touch: class III da neuron axons project into the
545 VNC in an anterior-posterior pattern. Axons from the T1 segment constitute the anterior-most T1
546 bundle within the VNC. The T1 and T2 axon bundles are injured by targeting the nerve bundles
547 right before they enter the commissure region, as marked by the red dots. Gentle-touch response
548 is then performed by stimulating the T1 or T2 segments using an eyelash. A total of four trials
549 are scored for each genotype. PC, pseudocephalon; T, thoracic; A, abdominal. **(b)** *mus101^A*
550 mutants show enhanced gentle-touch response after VNC injury, as shown by the Recovery
551 percentage. A larva is defined as showing recovery if the scores from at least two of the four
552 trials are 1 or above. While WT largely fail to respond even at 48 h AI, significantly more

553 *mus101^A* mutants show recovery as early as 24 h AI. **(c)** Gentle-touch response scores at 8, 24
554 and 48 h AI with various stimulation intensity. *Mus101^A* mutants display significantly higher
555 recovery especially with the T+++ stimulus. **(d)** Class III da neuron specific knockdown of
556 Rad17 mildly increases Recovery percentage at 48 h AI. **(e)** Class III da neuron specific
557 knockdown of Rad17 improves response scores at 48 h AI. **(f)** *mei41^{29D}* mutation mildly
558 increases Recovery percentage at 48 h AI. **(g)** *mei41^{29D}* mutation improves response scores at 48
559 h AI. *N* = 41 larvae for Ctrl, 23 for *mus101^A*, 33 for *mei41^{29D}*, 11, 26 and 26 for *Rad17 RNAi* at
560 8 h, 24 h and 48 h. **P* < 0.05, ***P* < 0.01, ****P* < 0.001 by Fisher's exact test (b, d and f), one-
561 way ANOVA followed by Tukey's test (c, e and g). See also Supplementary Fig. 6.

562

563 **Figure 5. Inhibiting the Atr pathway promotes synapse regeneration in flies.**

564 **(a)** Class III da neurons form cholinergic synapses in the VNC. Synaptotagmin-GFP
565 (syt.eGFP/syt) marks class III da neuron presynapses, which are tightly opposed by postsynaptic
566 cholinergic receptors labeled by α -bungarotoxin (α -BTX). Scale bar = 5 μ m. **(b)** In uninjured
567 class III da (C3da) neurons (marked in green), syt puncta (marked in red) are enriched at the
568 presynaptic terminals within the neuropil. Scale bar = 20 μ m. **(c)** *Mus101^A* mutants show
569 enhanced axon regeneration and synapse reformation in the CNS. Class III da neuron axon
570 bundles on one side of the VNC are ablated (dashed circles), resulting in the retraction of axons
571 out of the neuropil within 8 h AI. At 24 h AI, WT axons rarely regrow into the neuropil,
572 displaying retraction bulb like structures. *Mus101^A* mutant class III da neurons not only exhibit
573 extensive axon regeneration back into the neuropil, but also increase the percent of regenerating
574 axons containing syt puncta at the terminals (arrowheads), indicative of synapse reformation.
575 Two examples of *mus101^A* mutants are shown. The schematic drawings depict the VNC (blue),

576 neuropil (pink), uninjured axons (black), retracted axons (green) and regenerating axons (red).
577 Scale bar = 20 μm . **(d)** Quantification of axon and synapse regeneration. $N = 34$ and 35 axon
578 bundles from 8 and 10 larvae. The percent of regenerated axons increases from 21% in WT to
579 47% in *mus101A* mutants, $*P < 0.05$ by Fisher's exact test. The percent of regenerated axon
580 containing syt puncta is also increased in in *mus101A* mutants. See also Supplementary Fig. 6.

581

582 **Figure 6. ATR's response to osmotic stress depends on PIEZO1 and NOS.**

583 **(a to c)** Hypotonic stress-induced ATR clusters in the nucleus is attenuated in PIEZO1 knockout.
584 **(a)** Exogenously expressed FLAG-ATR is present in the cytoplasm in both WT and *PIEZO1KO*
585 HEK293T cells before treatment. 5 min or 7 min hypotonic stress induces robust clustering of
586 FLAG-ATR in the nucleus in WT cells, which is much attenuated in the *PIEZO1KO* cells. Fewer
587 cells produce the clusters. The clusters are smaller in size, fewer in number and lower in
588 intensity. The dashed circles outline the nucleus. Scale bar = 10 μm . **(b)** Quantification of the
589 fluorescence intensity of FLAG-ATR normalized to GFP shows a reduction in *PIEZO1KO* cells.
590 $N = 4, 8$ and 8 fields of view. **(c)** Quantification of the total area of FLAG-ATR clusters in the
591 nucleus per cell is also reduced in *PIEZO1KO* cells. $N = 36, 65$ and 70 cells. **(d to f)** ATR
592 clustering depends NOS. **(d)** Hypotonic stress-induced ATR clusters in WT HEK293T cells are
593 reduced by the NOS inhibitor 1400W dihydrochloride, while histamine, a NOS activator,
594 increases ATR clusters in *PIEZO1KO* cells. The dashed circles outline the nucleus. Scale bar =
595 10 μm . **(e)** Quantification of the fluorescence intensity of FLAG-ATR clusters. $N = 8$ fields of
596 view. **(f)** Quantification of the total area of FLAG-ATR clusters in the nucleus per cell. $N = 86,$
597 94, 87 and 97 cells. $*P < 0.05$, $**P < 0.01$, $***P < 0.001$ by two-tailed unpaired Student's t-test
598 **(b and c)**, One-way ANOVA followed by Tukey's multiple comparisons test **(e and f)**.

599

600 **Figure 7. Atr/mei41 functions downstream of Piezo and Nos in inhibiting axon**
601 **regeneration, and NO imaging.**

602 (a) Genetic interaction and epistasis analyses among *Piezo*, *Nos* and *Atr/mei41*. While class III
603 da neuron axons in *Nos^{Δ15}* heterozygotes, or transheterozygotes of *PiezoKO* and *mei41^{29D}*
604 (*mei41^{29D/+}*; *PiezoKO/+*) behave similarly to WT, significant enhancement of regeneration is
605 observed in transheterozygotes of *Nos^{Δ15}* and *mei41^{29D}* (*mei41^{29D/+}*; *Nos^{Δ15/+}*). Class III da
606 neuron specific overexpression of *grp* in *PiezoKO* or *Nos^{Δ15}* mutants reduces their regeneration
607 enhancement phenotype. On the other hand, Class III da neuron specific overexpression of
608 mPiezo-TriM or *Nos* fails to suppress the regeneration enhancement in *mei41^{29D}* mutants. The
609 injury site is demarcated by the dashed circle. Arrow marks axon stalling while arrowheads show
610 the regrowing axon tips. (b, c) Quantifications of class III da neuron axon regeneration with
611 Regeneration percentage (b) and Regeneration index (c). $N = 37, 8, 26, 24, 49, 31, 43, 22, 23, 22$
612 and 27 neurons from 3 to 14 larvae. (d to g) NO imaging in WT, *Nos^{Δ15}* mutants or *PiezoKO* at
613 48 h AI. (d) NO production is detected by DAF-FM diacetate. While in WT, NO is present
614 around the injured axon tip, along the axon and in the cell body, the fluorescence signal is
615 drastically reduced in *Nos^{Δ15}* mutants which lacks the NO producing enzyme. (e) The NO
616 fluorescence signal is similarly reduced in *PiezoKO*. The injury site is demarcated by the dashed
617 circle. (f) NO fluorescence signal is rarely detected in uninjured control class III da neurons. At
618 48 h AI, 62.5% of the WT class III da neurons show obvious NO fluorescence signal, compared
619 to 25% in *PiezoKO* or *Nos^{Δ15}* mutants. (g) The mean NO fluorescence intensity measured at the
620 growth cone tip is also significantly reduced in *PiezoKO* or *Nos^{Δ15}* mutants. $N = 8, 12$ and 8
621 neurons from 3 to 4 larvae. * $P < 0.05$, ** $P < 0.01$, *** $P < 0.001$ by Fisher's exact test (b), one-

622 way ANOVA followed by Holm-Sidak's test (c) or Dunnett's test (g). Scale bar = 20 μm . See
623 also Supplementary Fig 7.

624

625 **Figure 8. Inhibition of the Atr pathway by pharmacological inhibitors or conditional**
626 **knockout promotes mammalian DRG neuron axon regeneration *in vitro* and *in vivo*, and**
627 **axon outgrowth on substrates of differing stiffness.**

628 (a to c) Pharmacological inhibition of Atr or Chek1 modestly enhances axon regeneration of rat
629 embryonic DRG neurons cultured in a microfluidic chamber, when applied after injury. (a)
630 Inhibiting Atr with AZD6738 (0.5 μM), Chek1 with VE 822 (80 nM) or MK8776 (0.2 μM)
631 accelerates axon regeneration when imaged at 18 h AI. The axons are labeled with α -Gap43
632 staining. The dashed line marks the front of the axon tips in Control. (b) The axon coverage area
633 is measured and normalized to the total width of the microgrooves. The values from the
634 inhibitor-treated groups are further normalized to the corresponding DMSO vehicle control
635 group in the same experiment. $N = 7, 5, 5$ and 5 experiments. (c) Enhanced axon regeneration is
636 visible at 5 h AI when Atr is inhibited with AZD6738. The axons are labeled with α -Tuj1
637 staining. Scale bar = 100 μm . (d) Injection of the Chek1 inhibitor MK8776 (final concentration:
638 ~ 0.3 μM) into fly larvae right after injury enhances class III da neuron axon regeneration,
639 compared to the PBS injected control. Arrow marks retracted axon tip and arrowheads mark the
640 regenerating axon. Scale bar = 20 μm . (e, f) Quantifications of class III da neuron axon
641 regeneration with Regeneration percentage (e) and Regeneration index (f). $N = 23$ and 24
642 neurons from 4 larvae. (g, h) *Atr cKO* enhances sensory axon regeneration *in vivo*. Analysis of
643 regeneration of sensory axons by SCG10 immunostaining at SNL D3. Shown are sample images
644 of regenerating sensory axons identified by SCG10 (g) and quantification (h). SCG10

645 immunofluorescence intensity was measured at different distal distances and normalized to that
646 at the lesion site as the regenerative index. Dashed line marks the lesion site. Scale bar = 100 μ m.
647 $N = 6$ mice for each genotype. (i, j) *Piezol cKO* increases adult DRG neuron axon outgrowth on
648 hydrogels of 1 kPa, but not 30 kPa. (i) Representative images of DRG neurons (stained with
649 the α -Tuj1 antibody) grown on substrates of different stiffness. Scale bar = 50 μ m. (j)
650 Quantification of total neurite length normalized to that of the control. $N = 37, 28, 29$ and 34
651 neurons. $*P < 0.05$, $**P < 0.01$ by Fisher's exact test (e), one-way ANOVA followed by Holm-
652 Sidak's test (b), two-tailed unpaired Student's t-test (f and j), or Two-way ANOVA followed by
653 Sidak's test (h).

654

655 ACKNOWLEDGEMENT

656 We thank E.J. Brown for the *Atr^{fl/fl}* mouse; T. T. Su for fly lines; Bloomington Stock Centre,
657 VDRC and FlyORF for fly stocks; Addgene and GenScript for plasmids; A. Patapoutian for the
658 *PIEZO1* knockout cell line; N. Yakubovich and P. O'Farrell for the twine antibody, members of
659 the Song lab for helpful discussions. Y. S. is a recipient of the National Institute of Neurological
660 Disorders and Stroke (NINDS) Pathway to Independence Award. This work was supported by an
661 IDDRC New Program Development Award (CHOP/Penn), an NINDS K99/R00 award
662 (R00NS088211) and an NIH grant (1R01NS107392) to Y.S.

663

664 AUTHOR CONTRIBUTIONS

665 Conceptualization, F.L., L.M., D.L. and Y.S.; Methodology, F.L., T.Y.L., L.M., Q.W., D.L.,
666 K.P., Y.H., P.A.J and Y.S.; Investigation, F.L., T.Y.L., L.M., Q.W., D.L., J.N., J.I.G., C.W.,
667 S.W., J.Q., S.T., M.B., P.R., G.M.T. and Y.S.; Writing – Original Draft, D.L. and Y.S.; Writing

668 – Review & Editing, F.L., T.Y.L., L.M., Q.W. and G.M.T.; Funding Acquisition, Y.S.;
669 Supervision, G.M.T. and Y.S..

670

671 **AUTHOR INFORMATION**

672 The authors declare no competing financial interests. Correspondence and requests for materials
673 should be addressed to Y.S. (songy2@email.chop.edu).

674 The datasets generated in the current study are available from the corresponding author on
675 reasonable request.

676

677 **METHODS**

678 **Fly stocks.** *19-12-Gal4*⁷², *repo-Gal80*⁷³, *mei41*^{29D} 19, *UAS-Cdk1.T14A.Y15F*²¹, *ppk-CD4-*
679 *tdGFP*⁷⁴, *ppk-Gal4*⁷⁴, *Cdk1*^{B47} 22, 23, *Cdk1*^{E1-23} 22, 23, *mei41::FLAG (PBac{fTRG01361.sfGFP-*
680 *TVPTBF}VK00002)*²⁴, *221-Gal4*⁷⁵, *UAS-His2Av RNAi*³¹, *RPA2*^{KG00759} 32, *RPA3*^{G0241} 33,
681 *DmPiezoKO*, *UAS-Piezo RNAi*^{v2796}⁷⁶, *nompC-QF*⁷⁷, *QUAS-mCD8GFP*⁷⁸, *QUAS-mtdTomato*⁷⁸,
682 *ChAT-Gal4*⁴⁰, *nompC-Gal4*⁷⁷, *UAS-synaptotagmin-eGFP*⁴¹, *Nos*^{Δ15} 79, *UAS-mPiezo1-TriM*¹⁷ and
683 *UAS-Nos*⁸⁰ have been previously described. *grp*^{A196} *P{neoFRT}40A*, *UAS-grp RNAi*^{BL27277},
684 *UAS-twe*, *UAS-stg*, *UAS-twe RNAi*^{BL33044}, *UAS-twe RNAi*^{BL36587}, *UAS-mus304*
685 *RNAi*^{BL61355}, *tefu*^{atm-6}, *tefu*^{atm-3}, *rad50*^{EP1}, *nbs*¹, *mus101*^A, *UAS-Claspin RNAi*^{BL32974} *Hus1-*
686 *like*^{M11259} and *ctrip*^{M114762} were from the Bloomington stock center. *UAS-me141 RNAi*, *UAS-grp*
687 *RNAi*^{v10076}, *UAS-Rpa-70 RNAi*^{v11210}, *UAS-Rpa-70 RNAi*^{v110368}, *UAS-Rpa2 RNAi*^{v102306},
688 *UAS-Rpa2 RNAi*^{v30570}, *UAS-Rpa3 RNAi*^{v101833}, *UAS-Rpa3 RNAi*^{v15380}, *UAS-mus304*
689 *RNAi*^{v46012}, *UAS-Rad17 RNAi*^{v103552}, *UAS-Rad17 RNAi*^{v44723}, *UAS-Rad1 RNAi*^{v103430},
690 *UAS-Rad1 RNAi*^{v12676}, *UAS-mus101 RNAi*^{v31431} and *UAS-Claspin RNAi*^{v34476} were from

691 VDRC. *UAS-RpA-70* was from FlyORF. To generate the *UAS-hATR-WT*, *UAS-hATR-KD*, *UAS-*
692 *hCHEK1*, *UAS-RPA2* and *UAS-RPA3* stocks, the entire coding sequences were cloned into the
693 pACU2 vector, and the constructs were then injected (Rainbow Transgenic Flies, Inc).
694 Randomly selected male and female larvae were used. Analyses were not performed blind to the
695 conditions of the experiments. In our study, we typically used one mutant plus one RNAi
696 knockdown, or two independent RNAi strains to confirm the phenotype of each candidate gene.
697 In addition, overexpression analysis was performed for critical genes.

698

699 **Mice.** *Atr^{fl/fl}*⁸¹ mice were generously provided by E.J. Brown (University of Pennsylvania).
700 *Advillin-CreER*⁸² and *Piezo1^{fl/fl}*⁸³ mice were obtained from Jackson Laboratories. All studies
701 and procedures involving animal subjects were performed under the approval of the Institutional
702 Animal Care and Use Committee (IACUC) at the Children's Hospital of Philadelphia. Four to
703 six week old *Avil-CreER/Atr^{+/+}*, *Avil-CreER/Atr^{fl/+}* and *Avil-CreER/Atr^{fl/fl}*, or *Avil-*
704 *CreER/Piezo1^{+/+}*, *Avil-CreER/Piezo1^{fl/+}* and *Avil-CreER/Piezo1^{fl/fl}* mice were administered 2 mg
705 of tamoxifen daily by intraperitoneal injection for 5 consecutive days. SNL or DRG dissection
706 was performed approximately 2 weeks after the last tamoxifen injection. Genomic DNA from the
707 dorsal root ganglia was extracted at the end of an experiment and then analyzed by PCR to
708 confirm deletion. Age-matched mice were randomly assigned to experimental groups. Analyses
709 were not performed blind to the conditions of the experiments. All mice were housed in an
710 animal facility and maintained in a temperature controlled and light controlled environment with
711 an alternating 12 hours light/dark cycle. Up to 5 mice of the same sex from the same litter were
712 housed in a cage. The animals had no prior history of drug administration, surgery or behavioral
713 testing.

714

715 **Sensory axon lesion in *Drosophila*.** Da neuron axon lesion and imaging in the PNS or within
716 the VNC were performed in live fly larvae as previously described^{11, 12, 84}.

717

718 **Quantitative analyses of sensory axon regeneration in flies.** Quantification was performed as
719 previously described^{11, 12}. Briefly, for axon regeneration in the PNS, we used “Regeneration
720 percentage”, which depicts the percent of regenerating axons among all the axons that were
721 lesioned; “Regeneration length”, which measures the increase of axon length; “Regeneration
722 index”, which is calculated as an increase of “axon length”/“distance between the cell body and
723 the axon converging point (DCAC)” (Supplementary Fig. 1a). An axon is defined as
724 regenerating only when it obviously regenerated beyond the retracted axon stem, and this was
725 independently assessed of the other parameters. The regeneration parameters from various
726 genotypes were compared to that of the WT if not noted otherwise, and only those with
727 significant difference were labeled with the asterisks.

728

729 **Live imaging in flies.** Live imaging was performed as described^{85, 86}. Embryos were collected
730 for 2-24 hours on yeasted grape juice agar plates and were aged at 25°C or room temperature. At
731 the appropriate time, a single lava was mounted in 90% glycerol under coverslips sealed with
732 grease, imaged using a Leica SP8 or Zeiss LSM 880 microscope, and returned to grape juice agar
733 plates between imaging sessions.

734

735 **Behavioral assay.** We used *NompC-Gal4/+; NompC-QF, QUAS-CD8GFP/+* larvae as control;
736 *NompC-Gal4/UAS-Rad17 RNAiv103552; NompC-QF, QUAS-CD8GFP/UAS-Dcr2* for testing

737 *Rad17* knockdown, *mus101^A*; *NompC-Gal4/+*; *NompC-QF,QUAS-CD8GFP/+* for testing
738 *mus101* mutants, and *mei41^{29D}*; *NompC-Gal4/+*; *NompC-QF,QUAS-CD8GFP/+* for testing
739 *mei41* mutants. Larvae were raised at 25°C and 70% humidity. At 72 h AEL, larvae were injured
740 at the sites shown in Figure 4A. After injury, larvae were kept on grape agar plates at 25°C until
741 analysis.

742 The behavioral assay for the specific segments was modified from the method described
743 previously³⁸. Briefly, an eyelash was used for delivering the gentle-touch stimulus. Based on the
744 contact area between the eyelash and larval body wall, the gentle-touch stimulus was
745 subcategorized into touch+, touch++ and touch+++ (Supplementary Fig. 6a). For each larva, the
746 injured segments (T1 and T2) were stimulated by the eyelash with touch+, touch++ and
747 touch+++, respectively (4 trials for each stimulus), followed by testing of the uninjured segments
748 (T3 and A1). The scores were recorded as “1”, if stop (hesitate); “2”, if recoil or turn; “3”, if one
749 step back (single reverse contractile wave); “4”, if two or more steps back (multiple waves of
750 reverse contraction); “0”, if no response (Supplementary Fig. 6b). Only those larvae that showed
751 impaired response when stimulated at the T1 and T2 segments at 8 h AI, but retained normal
752 response at T3 and A2 segments were scored. If an injured larva scored >0 in at least two of the
753 four trials, it was defined as showing functional recovery. WT larvae showed no recovery at 24 h
754 AI and only limited recovery at 48 h AI.

755

756 **Immunohistochemistry.** Third instar larvae or cultured neurons were fixed according to
757 standard protocols. The following antibodies were used: mouse anti-p-His2Av antiserum
758 (UNC93-5.2.1, 1:100, Developmental Studies Hybridoma Bank), mouse Anti-FLAG M2 (F3165,
759 1:500, Sigma), rabbit anti-twe (1:100, O’Farrell Lab), mouse anti-Tuj1 (801202, 1:5000,

760 BioLegend), rabbit anti-Atrip (PA1-519, 1:400, ThermoFisher), rabbit anti-Chek1 (AV32589,
761 1:100, Sigma), rabbit anti-TopBP1 (LS-C663420-20, 1:1000, LSBio), α -bungarotoxin, Alexa-
762 594 conjugate (B13423, 5 μ g/mL, ThermoFisher), rabbit anti-Gap43 (NB300-143, 1:1000,
763 Novus Biologicals), rabbit anti-SCG10 (NBP1-49461, 1:5000, Novus Biologicals), DAPI
764 (D9542, 1:1000, Sigma) and fluorescence-conjugated secondary antibodies (1:1000, Jackson
765 ImmunoResearch).

766

767 **Quantitative RT-PCR and genotyping of *Hus1-like* insertion.** Quantitative PCR (q-PCR) was
768 done for *Hus1-like* and *rp49* according to the manufacturer's protocols. The primer sequences
769 were as follows: *Hus1-like qPCR F* 5'-agcacttcaactccctaacg-3', *Hus1-like qPCR R* 5'-
770 ccacatcctgtcgtacatcg-3', *rp49 qPCR F* 5'-cagtcggatcgatgctaaagctg-3' and *rp49 qPCR R* 5'-
771 taaccgatgtgggcatcagatac-3'. The primers for *Hus1-like* genotyping were: *Genotyping primer F*
772 5'-gaagtggcgcacgatgtccag-3' and *Genotyping primer R* 5'-actactcccgaaaaccgcttct-3'.

773

774 **Cell Culture, transfection, treatment and quantifications.** WT or *PIEZO1KO* (5E3)⁴³
775 HEK293T cells were maintained in DMEM medium supplemented with 10% FBS. Cells were
776 transfected with pcDNA3-FLAG-ATR and GFP (pLL3.7) in the presence of Lipofectamine 2000
777 (Invitrogen). 48 hours after transfection, cells were exposed to mock or hypotonic medium
778 (medium diluted 1: 5 with ddH₂O) for 5-7 min. In some conditions, 1400W dihydrochloride
779 (100 μ M, Santa Cruz) as a NOS inhibitor, or histamine (100 μ M, Santa Cruz) as a NOS activator,
780 were added to the hypotonic medium. For immunocytochemistry, fixed with 4% PFA for 20 min,
781 and stained with FLAG antibody. For fluorescence intensity quantification, the integrated
782 intensity of the whole 8-bit image was measured with ImageJ, and the FLAG-ATR fluorescence

783 intensity was normalized to that of GFP. For FLAG-ATR cluster analysis, DAPI was used to
784 define the nuclear area, and the total area of FLAG-ATR clusters per cell was measured using
785 the Analyze Particles plugin (Image J).

786

787 **NO imaging.** NO production was detected by DAF-FM diacetate (4-amino-5-methylamino-2',7'-
788 difluorofluorescein diacetate) (D23844, ThermoFisher). Fly larvae were dissected at 24 or 48 h
789 AI in PBS to expose the sensory neurons. The larval body wall – fillet prep was incubated in 10
790 μ M DAF-FM diacetate for 10 min at room temperature, rinsed in PBS, fixed with 4%
791 paraformaldehyde, rinsed in PBS, and imaged by confocal microscopy. DAF-FM diacetate
792 fluorescence was quantified in ImageJ by measuring the mean gray value around the injured
793 axon tip subtracting the background fluorescence.

794

795 **Microfluidic neuron culture and axotomy.** Methods were as previously described⁸⁷. Briefly, a
796 microfluidic culture chamber with several compartments was made using soft lithography in
797 PDMS. The axon compartment and somal compartment were separated by micrometer-sized
798 grooves. Dissociated DRG neurons from E16 rats were plated into the somal compartment. After
799 7 DIV (*days in vitro*), neurons in the somal compartment extend axons through the micro-
800 grooves and reach the axon compartment. Axotomy was performed by aspiration of the axon
801 compartment. Atr or Chek1 inhibitors were then added to the culture medium and neurons were
802 cultured for another 5 or 18 hours within the device, after which cells were fixed and stained
803 with the indicated antibodies.

804 Quantitative analysis of axon regrowth was performed as described previously¹⁷. In brief,
805 axons in the terminal chamber labeled by Gap43 staining were imaged using a Zeiss LSM880

806 laser scanning microscope with a 40× objective. Axon coverage area was calculated by
807 connecting the tips of the distal axons. Axon coverage area was normalized to the length of the
808 microgrooves to obtain the Normalized regeneration.

809

810 **Fly larvae injection.** MK8776 (S2735, selleckchem, 5 mM stock in DMSO) was dissolved in
811 PBS before using. It was injected into larvae right after injury to a final concentration of ~0.3 μM.
812 The final concentration of the chemical injected into larvae was calculated based on the volume
813 estimated from larvae weight. Injection of PBS with the corresponding DMSO was the vehicle
814 control. Injection was performed by glass micropipettes and Hamilton syringes.

815

816 **Sciatic nerve lesion (SNL) and quantification of sensory axon regeneration.** Mice (6 to 8
817 weeks old) were anesthetized and a small incision was made on the skin at the mid-thigh level.
818 The sciatic nerve with its three major branches was exposed through a gluteal muscle splitting
819 incision. In the sham control mouse, the posterior tibial nerve was exposed and elevated from its
820 tissue bed, but no crush lesion was performed. In the experimental groups, the nerve crush lesion
821 was performed on the posterior tibial nerve by freeing the nerve from connective tissue and fully
822 crushed for 10 s. The muscle layer was closed with a 5-0 chromic gut sutures (Ethicon Inc., NJ)
823 and the skin were closed with Autoclip® system (F.S.T. Instruments, CA).

824 Three days after surgery, mice were deeply anesthetized with 200 mg/kg ketamine given
825 intraperitoneally followed by exsanguination by trans-cardiac perfusion with PBS (0.01M, pH
826 7.4) and fixation by paraformaldehyde (4% PFA in PBS, pH 7.4). Whole DRG (lumbar L3-L5)
827 and full length sciatic nerve were dissected and post-fixed for 24 h and cryoprotected in sucrose
828 solution (30% sucrose in 0.01M PBS, pH 7.4) at 4°C. Fixed DRG and sciatic nerve tissues were

829 embedded in Optimal Cutting Temperature O.C.T Compound (Leica, Germany) and sectioned at
830 14 μm using Leica CM3050 (Leica, Germany). DRGs was later processed as floating sections
831 and sagittal sciatic nerve sections were thaw-mounted on gelatin-dodecahydrate treated glass
832 microscope slides (Superfrost Plus, Fisher Scientific).

833 To measure regeneration of the sciatic nerve, sections were stained with the α -SCG10
834 antibody. SCG10 intensity was measured by ImageJ and the average intensities were calculated
835 across 100 μm non-overlapping regions and normalized. The regenerative index was calculated
836 as previously described⁸⁸.

837

838 **Stiffness assay.** Polyacrylamide (PAA) hydrogels were made as described by^{57, 89} with some
839 modifications. Briefly, 18 mm circular glass coverslips (NeuViro, Vancouver, WA) were treated
840 with 3-aminopropyl-trimethoxysilane (Fisher Scientific), extensively washed with Milli-Q H₂O,
841 and treated with 0.5% glutaraldehyde (Fisher Scientific). Rectangular 22 x 50 mm glass
842 coverslips (Fisher Scientific) were treated with hydrocarbon soluble siliconizing solution to
843 make non-adhesive top coverslips. Next, 40% Acrylamide and 2% bis-acrylamide (Bio-Rad
844 Laboratories, Richmond, CA) were mixed at ratios of 5%, 0.1% and 12%, 0.4% to achieve gels
845 of 1.0 and 30.0 kPa stiffnesses, respectively⁸⁹. Polymerization was initiated by adding
846 ammonium persulfate (APS, stock concentration of 10% w/v, ThermoFisher) and N,N,N,N-
847 tetramethylethylenediamine (TEMED, AcrosOrganics, Morris Plains, NJ). After initiation, 80
848 μL of gel solution was transferred to each siliconized (bottom) coverslip and covered with the
849 nonadhesive top coverslip. After 15 minutes, the bottom coverslips were removed, revealing
850 hydrogels attached to only the top coverslip. Gels were allowed to swell in Milli-Q H₂O for 1 h
851 at 37°C and coated in sulfosuccinimidyl6-(40 -azido-20 -nitrophenylamino) hexanoate (sulfo-

852 SANPAH, ThermoFisher) and photoactivated with 365 nm UV light for 10 minutes. PAA gels
853 were gently washed with Milli-Q H₂O and coated in 0.1 mg/mL Poly-L-Lysine overnight in a
854 37°C, 5% CO₂, and humidity-controlled incubator. On the day of cell seeding, the PAA gels
855 were coated in 5 µg/mm² laminin (20 µL of 1 mg/mL laminin in 1000 mL growth medium) for 6
856 hours, 37°C.

857 DRG primary culture was performed according to⁵⁶. Briefly, anesthetized mice were
858 perfused with chilled, sterile PBS, and DRGs were dissected and washed in cold HBSS. DRG
859 tissues were digested and incubated for 21 minutes at 37°C in a solution containing 1 mg L-
860 cysteine (Sigma-Aldrich), 60U Papain (Worthington Biochemical Corporation), 1 µg DNase I
861 (Fisher Scientific) in 1.5 mL Ca²⁺/Mg²⁺-free HBSS. The DRG tissues were pelleted (250x g, 3
862 minutes, room temperature) and resuspended and further digested (37°C, 20 minutes) in an
863 enzyme cocktail containing 15 mg dispase II (Sigma-Aldrich) and 12 mg of collagenase
864 (Worthington Biochemical Corporation) in 3 mL of Ca²⁺/Mg²⁺-free HBSS. The
865 dispase/collagenase solution was inactivated by the addition of a 1:1 ratio of tissue solution to
866 prewarmed Neurobasal A medium (1x Glutamax, B27 supplement, 10% FBS). The cell solution
867 was passed through a 70 µm cell strainer (ThermoFisher), pelleted (250x g, 3 minutes, room
868 temperature), and resuspended in culture medium (Neurobasal A, B27, Glutamax, 10% FBS, 100
869 ng/mL neural growth factor; mouse NGF 7.0s, Millipore Sigma). DRG neurons were then seeded
870 on each corresponding PAA hydrogel at approximately 30,000 cells per 250 mm² growth area to
871 achieve single cell density. Primary DRG neurons were cultured on PAA gels for 38-40 hours
872 before fixed in pre-warmed 4% sucrose/4% PFA in 1x PBS for 10 minutes at room temperature.
873 Cells were permeabilized in 0.2% Triton X-100 in TBS (10 minutes, room temperature) and

874 blocked in 10% normal donkey serum in PBS (2 h, room temperature) and stained with α -Tuj1
875 antibody.

876 Neurons were imaged on a Zeiss LSM 880 confocal laser scanning microscope and
877 image acquisition occurred within 48 hours of mounting each hydrogel. Each image's maximum
878 projection image was used during analysis of neurite lengths. The total neurite length was
879 measured with ImageJ's plugin program, "Simple Neurite Tracer"⁹⁰, and normalized to the mean
880 of the control.

881

882 **Quantification and statistical analysis.** No statistical methods were used to pre-determine
883 sample sizes but our sample sizes are similar to those reported in previous publications^{11, 12}, and
884 the statistical analyses were done afterwards without interim data analysis. Data distribution was
885 assumed to be normal but this was not formally tested. All data were collected and processed
886 randomly. Each experiment was successfully reproduced at least three times and was performed
887 on different days. The values of "N" (sample size) are provided in the figure legends. Data are
888 expressed as mean \pm SEM in bar graphs. No data points were excluded. Two-tailed unpaired
889 Student's t-test was performed for comparison between two groups of samples. One-way
890 ANOVA followed by multiple comparison test was performed for comparisons among three or
891 more groups of samples. Two-way ANOVA followed by multiple comparison test was
892 performed for comparisons between two or more curves. Fisher's exact test was used to compare
893 the percentage. Statistical significance was assigned, * $P < 0.05$, ** $P < 0.01$, *** $P < 0.001$.

894

895 **SUPPLEMENTARY INFORMATION**

896 Supplementary Figures 1-8

897 Supplementary Videos 1-6

898

899 **SUPPLEMENTARY FIGURE LEGENDS**

900 **Supplementary Figure 1. Related to Figure 1. Quantification of sensory axon regeneration**
901 **in the fly PNS, dendrite branching and mei41 expression.**

902 (a) “Regeneration index” is calculated as an increase of “axon length”/“distance between the cell
903 body and the axon converging point (DCAC)”. (b) The dendrite of class III da neuron of various
904 genotypes were traced at 72 h AI and the total dendrite length was quantified. $N = 20, 15, 15$ and
905 10 neurons from 3 to 5 larvae. (c) Expression and localization of mei41 with and without injury.
906 Mei41 is present mainly in the nucleus of class III da sensory neurons. No significant difference
907 is observed after axon injury. The injury site is demarcated by the green dashed circle. Class III
908 and IV da neurons are outlined by the red and yellow dashed lines, respectively. $N = 8$ segments
909 from 4 larvae. No statistical difference is detected by One-way ANOVA followed by Dunnett’s
910 test (b).

911

912 **Supplementary Figure 2. Related to Figure 2. The Atm/tefu pathway does not regulate**
913 **axon regeneration in da sensory neurons in flies, and class I da neuron axon regeneration.**

914 (a, b) Inhibiting the Atm/tefu pathway does not significantly alter class IV da neuron axon
915 regeneration. Quantifications of class IV da neuron axon regeneration with Regeneration
916 percentage (a) and Regeneration index (b). $N = 27, 17, 19$ and 18 neurons from 5 to 7 larvae. (c
917 to e) Atm/tefu loss of function does not promote class III da neuron axon regeneration. (c)
918 Atm/tefu removal as in *tefu^{atm-6/atm-3}* mutants does not increase axon regeneration. The injury site
919 is demarcated by the dashed circle. Arrow marks axon stalling. Scale bar = 20 μm .

920 Quantifications of class III da neuron axon regeneration with Regeneration percentage (d) and
921 Regeneration index (e), shown in the scatter plot. $N = 23$ and 22 neurons from 7 to 8 larvae. No
922 statistical difference is detected by Fisher's exact test (a and d), one-way ANOVA followed by
923 Dunnett's test (b), two-tailed unpaired Student's t-test (e). **(f to h)** *PiezoKO* and *mei41^{29D}*
924 mutants enhance class I da neuron axon regeneration. The injury site is demarcated by the dashed
925 circle. Arrowheads mark regenerating axons. Scale bar = 20 μm . Quantifications of class I da
926 neuron axon regeneration with Regeneration percentage (g) and Regeneration index (h). $N = 40$,
927 31 and 26 neurons from 7 to 11 larvae. $*P < 0.05$, $**P < 0.01$ by Fisher's exact test (g), one-way
928 ANOVA followed by Dunnett's test (h).

929

930 **Supplementary Figure 3. Related to Figure 2. Overexpression of RPAs does not reduce**
931 **axon regeneration.**

932 Quantifications of class IV da neuron axon regeneration with Regeneration percentage (a) and
933 Regeneration index (b). $N = 31$, 29, 26 and 24 neurons from 7 to 8 larvae. No statistical
934 difference is detected by Fisher's exact test (a), one-way ANOVA followed by Dunnett's test (b).

935

936 **Supplementary Figure 4. Related to Figure 3. The insertional allele of Hus1-like – Hus1-**
937 **like^{M11259} is a loss of function mutant, and *ctrip* mutants do not show increased axon**
938 **regeneration.**

939 **(a)** The *Hus1-like^{M11259}* insertional locus, and primers for genotyping and quantitative RT-PCR.

940 **(b)** Genomic PCR using the genotyping primers confirms the insertion. **(c)** Quantitative RT-PCR

941 shows significant reduction of the *Hus1-like* transcripts in the *Hus1-like^{M11259}* mutants. *rp49* was

942 used as the loading control, and the *Hus1-like* mRNA level was normalized to that of WT. $N = 3$

943 biological replicates from 5-10 larvae each. $*P < 0.05$, by two-tailed unpaired Student's t-test.

944 **(d)** Quantifications of class III da neuron axon regeneration with Regeneration percentage and
945 Regeneration index. $N = 23$ and 27 neurons from 6 to 7 larvae. No statistical difference is
946 detected by Fisher's exact test or two-tailed unpaired Student's t-test.

947

948 **Supplementary Figure 5. Related to Figure 3. The expression pattern of Atr pathway**
949 **members in fly, mouse and human.**

950 **(a)** Expression and localization of twe with or without injury. Twe is present mainly in the
951 nucleus of class III da sensory neurons. No significant difference is observed after axon injury.
952 The injury site is demarcated by the green dashed circle. Class III da neuron cell bodies are
953 outlined by the red dashed circle. Twe is also expressed in other da neurons. Scale bar = $20 \mu\text{m}$.

954 **(b)** Immunostaining for Atrip, Chek1 and TopBP1 using mouse DRG tissue sections. All three
955 are expressed with or without sciatic nerve lesion (SNL). DRG neurons were counterstained with
956 the α -Tuj1 antibody. Scale bar = $20 \mu\text{m}$. **(c)** Expression level of Atr pathway members in
957 various tissues in mouse and human. All of them are expressed in the mouse and human DRG,
958 although at a low to median level.

959

960 **Supplementary Figure 6. Related to Figures 4 and 5. The modified gentle-touch behavioral**
961 **paradigm for assessing functional recovery after CNS injury in flies.**

962 **(a)** The definition of the gentle-touch stimulus. The intensity of the stimulation is subcategorized
963 based on the contact area between the eyelash and the body segment: touch+, touch++ and
964 touch+++, with the eyelash diameter covering $<1/8$, $1/8-1/4$ or $1/4-1/2$ of the segment,
965 respectively. **(b)** The scoring system for the gentle-touch response – gently touching larval

966 anterior segments with an eyelash elicits a set of stereotypical response. While the larvae are
967 moving forward, by gentle touch, if they stop (hesitate), score 1; recoil or turn, score 2; one step
968 back (single reverse contractile wave), score 3; two or more steps back (multiple waves of
969 reverse contraction), score 4; no response, score 0. (c) Injuring the class III da neuron axon
970 bundle at T1 or T2 in the VNC leads to impaired touch response specifically at segment T1 or
971 T2, without affecting neighboring segments. Total response scores from 4 trials are added and
972 shown in scatter plots. $N = 10$ larvae. (d to f) The behavioral response in the uninjured T3 and
973 A1 segments are comparable among the different genotypes – *mus101^A* mutants (d), class III da
974 neuron specific *Rad17 RNAi* (e) and *mei41^{29D}* mutants (f). Larvae also show a graded response
975 according to the stimulation intensity. $N = 41$ larvae for Ctrl, 23 for *mus101^A*, 33 for *mei41^{29D}*,
976 11, 26 and 26 for *Rad17 RNAi* at 8 h, 24 h and 48 h. $*P < 0.05$, $**P < 0.01$, $***P < 0.001$ by
977 one-way ANOVA followed by Tukey's test (c to f). (g) Class III da neurons are co-labeled by
978 *nompC-QF>mCD8GFP* (the class III da neuron marker) and *ChAT-Gal4>CD4TdTomato*.
979 Arrowhead marks the class III da neuron cell body. Scale bar = 20 μm .

980

981 **Supplementary Figure 7. Related to Figure 7. NO imaging in uninjured class III da**
982 **neurons does not show significant difference among WT, *PiezoKO* and *Nos^{Δ15}* mutants.** No
983 obvious NO fluorescence signal is detected in uninjured class III da neurons. $N = 8, 12$ and 8
984 neurons from 3 to 4 larvae. Scale bar = 20 μm .

985

986 **Supplementary Figure 8. The proposed Piezo-Nos-Atr-Chek1 pathway in inhibiting axon**
987 **regeneration.** The proposed Piezo-Nos-Atr-Chek1 signaling cascade that inhibits axon
988 regeneration. During axon regeneration, the mechanical force resulting from the interactions

989 between the growth cone and the environment, activates the mechanosensitive ion channel Piezo
990 at the growth cone tip, leading to local calcium influx and activation of Nos, which then
991 produces NO. NO functions as a second messenger and propagates to the nucleus where it
992 activates Atr and the associated checkpoint complex. Atr then phosphorylates and activates
993 Chek1, which phosphorylates and inactivates Cdc25, inhibiting its ability to dephosphorylate and
994 activate Cdk1. The phosphorylated and inactive Cdk1 suppresses axon regeneration through
995 downstream effectors.

996

997 **Supplementary Videos 1-6. The gentle-touch behavioral assay for assessing functional**
998 **recovery after CNS injury.**

999 **Supplementary Video 1. Related to Figure 4 and Supplementary Figure 6. WT 8 h AI**

1000 **Supplementary Video 2. Related to Figure 4 and Supplementary Figure 6. WT 48 h AI**

1001 **Supplementary Video 3. Related to Figures 4 and Supplementary Figure 6. *Mus101^A***
1002 **mutants 8 h AI**

1003 **Supplementary Video 4. Related to Figures 4 and Supplementary Figure 6. *Mus101^A***
1004 **mutants 48 h AI**

1005 **Supplementary Video 5. Related to Figures 4 and Supplementary Figure 6. Class III da**
1006 **neuron specific *Rad17* RNAi 8 h AI**

1007 **Supplementary Video 6. Related to Figures 4 and Supplementary Figure 6. Class III da**
1008 **neuron specific *Rad17* RNAi 48 h AI**

1009

1010 REFERENCES

1011 1. Liu, K., Tedeschi, A., Park, K.K. & He, Z. Neuronal intrinsic mechanisms of axon
1012 regeneration. *Annu Rev Neurosci* **34**, 131-152 (2011).

- 1013 2. Di Giovanni, S. Molecular targets for axon regeneration: focus on the intrinsic pathways.
1014 *Expert Opin Ther Targets* **13**, 1387-1398 (2009).
- 1015 3. Schwab, M.E. & Strittmatter, S.M. Nogo limits neural plasticity and recovery from
1016 injury. *Curr Opin Neurobiol* **27**, 53-60 (2014).
- 1017 4. Tedeschi, A. & Bradke, F. Spatial and temporal arrangement of neuronal intrinsic and
1018 extrinsic mechanisms controlling axon regeneration. *Curr Opin Neurobiol* **42**, 118-127
1019 (2017).
- 1020 5. Mahar, M. & Cavalli, V. Intrinsic mechanisms of neuronal axon regeneration. *Nat Rev*
1021 *Neurosci* **19**, 323-337 (2018).
- 1022 6. Terzis, J.K. & Kokkalis, Z.T. Selective contralateral c7 transfer in posttraumatic brachial
1023 plexus injuries: a report of 56 cases. *Plast Reconstr Surg* **123**, 927-938 (2009).
- 1024 7. Songcharoen, P., Wongtrakul, S., Mahaisavariya, B. & Spinner, R.J. Hemi-contralateral
1025 C7 transfer to median nerve in the treatment of root avulsion brachial plexus injury. *J*
1026 *Hand Surg Am* **26**, 1058-1064 (2001).
- 1027 8. Lundborg, G. A 25-year perspective of peripheral nerve surgery: evolving neuroscientific
1028 concepts and clinical significance. *J Hand Surg Am* **25**, 391-414 (2000).
- 1029 9. Painter, M.W. *et al.* Diminished Schwann cell repair responses underlie age-associated
1030 impaired axonal regeneration. *Neuron* **83**, 331-343 (2014).
- 1031 10. He, Z. & Jin, Y. Intrinsic Control of Axon Regeneration. *Neuron* **90**, 437-451 (2016).
- 1032 11. Song, Y. *et al.* Regeneration of Drosophila sensory neuron axons and dendrites is
1033 regulated by the Akt pathway involving Pten and microRNA bantam. *Genes Dev* **26**,
1034 1612-1625 (2012).
- 1035 12. Song, Y. *et al.* Regulation of axon regeneration by the RNA repair and splicing pathway.
1036 *Nat Neurosci* **18**, 817-825 (2015).
- 1037 13. Fulda, S., Gorman, A.M., Hori, O. & Samali, A. Cellular stress responses: cell survival
1038 and cell death. *Int J Cell Biol* **2010**, 214074 (2010).
- 1039 14. Donzelli, M. & Draetta, G.F. Regulating mammalian checkpoints through Cdc25
1040 inactivation. *EMBO Rep* **4**, 671-677 (2003).
- 1041 15. Zou, L. Single- and double-stranded DNA: building a trigger of ATR-mediated DNA
1042 damage response. *Genes Dev* **21**, 879-885 (2007).
- 1043 16. Kumar, A. *et al.* ATR mediates a checkpoint at the nuclear envelope in response to
1044 mechanical stress. *Cell* **158**, 633-646 (2014).
- 1045 17. Song, Y. *et al.* The Mechanosensitive Ion Channel Piezo Inhibits Axon Regeneration.
1046 *Neuron* (2019).
- 1047 18. Syeda, R. *et al.* Piezo1 Channels Are Inherently Mechanosensitive. *Cell Rep* **17**, 1739-
1048 1746 (2016).
- 1049 19. Laurencon, A., Purdy, A., Sekelsky, J., Hawley, R.S. & Su, T.T. Phenotypic analysis of
1050 separation-of-function alleles of MEI-41, Drosophila ATM/ATR. *Genetics* **164**, 589-601
1051 (2003).
- 1052 20. Lee, T. & Luo, L. Mosaic analysis with a repressible cell marker for studies of gene
1053 function in neuronal morphogenesis. *Neuron* **22**, 451-461 (1999).
- 1054 21. Ayeni, J.O. *et al.* Dual phosphorylation of cdk1 coordinates cell proliferation with key
1055 developmental processes in Drosophila. *Genetics* **196**, 197-210 (2014).
- 1056 22. Clegg, N.J., Whitehead, I.P., Williams, J.A., Spiegelman, G.B. & Grigliatti, T.A. A
1057 developmental and molecular analysis of Cdc2 mutations in Drosophila melanogaster.
1058 *Genome* **36**, 676-685 (1993).

- 1059 23. Stern, B., Ried, G., Clegg, N.J., Grigliatti, T.A. & Lehner, C.F. Genetic analysis of the
1060 *Drosophila cdc2* homolog. *Development* **117**, 219-232 (1993).
- 1061 24. Sarov, M. *et al.* A genome-wide resource for the analysis of protein localisation in
1062 *Drosophila*. *Elife* **5**, e12068 (2016).
- 1063 25. Silva, E. *et al.* ATM is required for telomere maintenance and chromosome stability
1064 during *Drosophila* development. *Curr Biol* **14**, 1341-1347 (2004).
- 1065 26. Ciapponi, L. *et al.* The *Drosophila* Mre11/Rad50 complex is required to prevent both
1066 telomeric fusion and chromosome breakage. *Curr Biol* **14**, 1360-1366 (2004).
- 1067 27. Bi, X. *et al.* *Drosophila* ATM and ATR checkpoint kinases control partially redundant
1068 pathways for telomere maintenance. *Proc Natl Acad Sci U S A* **102**, 15167-15172 (2005).
- 1069 28. Bonner, W.M. *et al.* GammaH2AX and cancer. *Nat Rev Cancer* **8**, 957-967 (2008).
- 1070 29. Kuo, L.J. & Yang, L.X. Gamma-H2AX - a novel biomarker for DNA double-strand
1071 breaks. *In Vivo* **22**, 305-309 (2008).
- 1072 30. Lake, C.M., Holsclaw, J.K., Bellendir, S.P., Sekelsky, J. & Hawley, R.S. The
1073 development of a monoclonal antibody recognizing the *Drosophila melanogaster*
1074 phosphorylated histone H2A variant (gamma-H2AV). *G3 (Bethesda)* **3**, 1539-1543
1075 (2013).
- 1076 31. Neely, G.G. *et al.* A genome-wide *Drosophila* screen for heat nociception identifies
1077 alpha2delta3 as an evolutionarily conserved pain gene. *Cell* **143**, 628-638 (2010).
- 1078 32. Crest, J., Oxnard, N., Ji, J.Y. & Schubiger, G. Onset of the DNA replication checkpoint
1079 in the early *Drosophila* embryo. *Genetics* **175**, 567-584 (2007).
- 1080 33. Zhou, L. & Luo, H. Replication protein a links cell cycle progression and the onset of
1081 neurogenesis in *Drosophila* optic lobe development. *J Neurosci* **33**, 2873-2888 (2013).
- 1082 34. Farrell, J.A. & O'Farrell, P.H. Mechanism and regulation of Cdc25/Twine protein
1083 destruction in embryonic cell-cycle remodeling. *Curr Biol* **23**, 118-126 (2013).
- 1084 35. Flegel, C. *et al.* RNA-Seq Analysis of Human Trigeminal and Dorsal Root Ganglia with
1085 a Focus on Chemoreceptors. *PLoS One* **10**, e0128951 (2015).
- 1086 36. Ray, P. *et al.* Comparative transcriptome profiling of the human and mouse dorsal root
1087 ganglia: an RNA-seq-based resource for pain and sensory neuroscience research. *Pain*
1088 **159**, 1325-1345 (2018).
- 1089 37. Hao, Y. & Collins, C. Intrinsic mechanisms for axon regeneration: insights from injured
1090 axons in *Drosophila*. *Curr Opin Genet Dev* **44**, 84-91 (2017).
- 1091 38. Kernan, M., Cowan, D. & Zuker, C. Genetic dissection of mechanosensory transduction:
1092 mechanoreception-defective mutations of *Drosophila*. *Neuron* **12**, 1195-1206 (1994).
- 1093 39. Yan, Z. *et al.* *Drosophila* NOMPC is a mechanotransduction channel subunit for gentle-
1094 touch sensation. *Nature* **493**, 221-225 (2013).
- 1095 40. Salvaterra, P.M. & Kitamoto, T. *Drosophila* cholinergic neurons and processes visualized
1096 with Gal4/UAS-GFP. *Brain Res Gene Expr Patterns* **1**, 73-82 (2001).
- 1097 41. Zhang, Y.Q., Rodesch, C.K. & Broadie, K. Living synaptic vesicle marker:
1098 synaptotagmin-GFP. *Genesis* **34**, 142-145 (2002).
- 1099 42. Couton, L. *et al.* Development of connectivity in a motoneuronal network in *Drosophila*
1100 larvae. *Curr Biol* **25**, 568-576 (2015).
- 1101 43. Dubin, A.E. *et al.* Endogenous Piezo1 Can Confound Mechanically Activated Channel
1102 Identification and Characterization. *Neuron* **94**, 266-270 e263 (2017).
- 1103 44. Garvey, E.P. *et al.* 1400W is a slow, tight binding, and highly selective inhibitor of
1104 inducible nitric-oxide synthase in vitro and in vivo. *J Biol Chem* **272**, 4959-4963 (1997).

- 1105 45. Lantoine, F., Iouzalén, L., Devynck, M.A., Millanvoye-Van Brussel, E. & David-
1106 Dufilho, M. Nitric oxide production in human endothelial cells stimulated by histamine
1107 requires Ca²⁺ influx. *Biochem J* **330** (Pt 2), 695-699 (1998).
- 1108 46. Wang, X., Zalcenstein, A. & Oren, M. Nitric oxide promotes p53 nuclear retention and
1109 sensitizes neuroblastoma cells to apoptosis by ionizing radiation. *Cell Death Differ* **10**,
1110 468-476 (2003).
- 1111 47. Jaszczak, J.S., Wolpe, J.B., Dao, A.Q. & Halme, A. Nitric Oxide Synthase Regulates
1112 Growth Coordination During *Drosophila melanogaster* Imaginal Disc Regeneration.
1113 *Genetics* **200**, 1219-1228 (2015).
- 1114 48. Jaszczak, J.S., Wolpe, J.B., Bhandari, R., Jaszczak, R.G. & Halme, A. Growth
1115 Coordination During *Drosophila melanogaster* Imaginal Disc Regeneration Is Mediated
1116 by Signaling Through the Relaxin Receptor Lgr3 in the Prothoracic Gland. *Genetics* **204**,
1117 703-709 (2016).
- 1118 49. Zhou, B. *et al.* Facilitation of axon regeneration by enhancing mitochondrial transport
1119 and rescuing energy deficits. *J Cell Biol* **214**, 103-119 (2016).
- 1120 50. Holland, S.M. *et al.* Palmitoylation controls DLK localization, interactions and activity to
1121 ensure effective axonal injury signaling. *Proc Natl Acad Sci U S A* **113**, 763-768 (2016).
- 1122 51. Weber, A.M. & Ryan, A.J. ATM and ATR as therapeutic targets in cancer. *Pharmacol*
1123 *Ther* **149**, 124-138 (2015).
- 1124 52. Manic, G., Obrist, F., Sistigu, A. & Vitale, I. Trial Watch: Targeting ATM-CHK2 and
1125 ATR-CHK1 pathways for anticancer therapy. *Mol Cell Oncol* **2**, e1012976 (2015).
- 1126 53. Daud, A.I. *et al.* Phase I dose-escalation trial of checkpoint kinase 1 inhibitor MK-8776
1127 as monotherapy and in combination with gemcitabine in patients with advanced solid
1128 tumors. *J Clin Oncol* **33**, 1060-1066 (2015).
- 1129 54. Weiss, G.J. *et al.* Phase I dose-escalation study to examine the safety and tolerability of
1130 LY2603618, a checkpoint 1 kinase inhibitor, administered 1 day after pemetrexed 500
1131 mg/m² every 21 days in patients with cancer. *Invest New Drugs* **31**, 136-144 (2013).
- 1132 55. Shin, J.E., Geisler, S. & DiAntonio, A. Dynamic regulation of SCG10 in regenerating
1133 axons after injury. *Exp Neurol* **252**, 1-11 (2014).
- 1134 56. Malin, S.A., Davis, B.M. & Molliver, D.C. Production of dissociated sensory neuron
1135 cultures and considerations for their use in studying neuronal function and plasticity. *Nat*
1136 *Protoc* **2**, 152-160 (2007).
- 1137 57. Kandow, C.E., Georges, P.C., Janmey, P.A. & Beningo, K.A. Polyacrylamide hydrogels
1138 for cell mechanics: steps toward optimization and alternative uses. *Methods Cell Biol* **83**,
1139 29-46 (2007).
- 1140 58. Koch, D., Rosoff, W.J., Jiang, J., Geller, H.M. & Urbach, J.S. Strength in the periphery:
1141 growth cone biomechanics and substrate rigidity response in peripheral and central
1142 nervous system neurons. *Biophys J* **102**, 452-460 (2012).
- 1143 59. Polackwich, R.J., Koch, D., McAllister, R., Geller, H.M. & Urbach, J.S. Traction force
1144 and tension fluctuations in growing axons. *Front Cell Neurosci* **9**, 417 (2015).
- 1145 60. Moeendarbary, E. *et al.* The soft mechanical signature of glial scars in the central nervous
1146 system. *Nat Commun* **8**, 14787 (2017).
- 1147 61. Yuan, Z. *et al.* Activation of FOXO1 by Cdk1 in cycling cells and postmitotic neurons.
1148 *Science* **319**, 1665-1668 (2008).
- 1149 62. Byrne, A.B. *et al.* Insulin/IGF1 signaling inhibits age-dependent axon regeneration.
1150 *Neuron* **81**, 561-573 (2014).

- 1151 63. Wynne, C.L. & Vallee, R.B. Cdk1 phosphorylation of the dynein adapter Nde1 controls
1152 cargo binding from G2 to anaphase. *J Cell Biol* **217**, 3019-3029 (2018).
- 1153 64. Ducommun Priest, M., Navarro, M.F., Bremer, J. & Granato, M. Dynein promotes
1154 sustained axonal growth and Schwann cell remodeling early during peripheral nerve
1155 regeneration. *PLoS Genet* **15**, e1007982 (2019).
- 1156 65. Blanquie, O. & Bradke, F. Cytoskeleton dynamics in axon regeneration. *Curr Opin*
1157 *Neurobiol* **51**, 60-69 (2018).
- 1158 66. Di Giovanni, S. *et al.* The tumor suppressor protein p53 is required for neurite outgrowth
1159 and axon regeneration. *EMBO J* **25**, 4084-4096 (2006).
- 1160 67. Byrne, A.B. *et al.* Inhibiting poly(ADP-ribosylation) improves axon regeneration. *Elife* **5**
1161 (2016).
- 1162 68. Wang, X. *et al.* Inhibition of Poly-ADP-Ribosylation Fails to Increase Axonal
1163 Regeneration or Improve Functional Recovery after Adult Mammalian CNS Injury.
1164 *eNeuro* **3** (2016).
- 1165 69. Martin, L.J., Chen, K. & Liu, Z. Adult motor neuron apoptosis is mediated by nitric oxide
1166 and Fas death receptor linked by DNA damage and p53 activation. *J Neurosci* **25**, 6449-
1167 6459 (2005).
- 1168 70. Kidiyoor, G.R., Kumar, A. & Foiani, M. ATR-mediated regulation of nuclear and cellular
1169 plasticity. *DNA repair* **44**, 143-150 (2016).
- 1170 71. Shanske, A., Caride, D.G., Menasse-Palmer, L., Bogdanow, A. & Marion, R.W. Central
1171 nervous system anomalies in Seckel syndrome: report of a new family and review of the
1172 literature. *American journal of medical genetics* **70**, 155-158 (1997).
- 1173 72. Xiang, Y. *et al.* Light-avoidance-mediating photoreceptors tile the Drosophila larval body
1174 wall. *Nature* **468**, 921-926 (2010).
- 1175 73. Awasaki, T., Lai, S.L., Ito, K. & Lee, T. Organization and postembryonic development of
1176 glial cells in the adult central brain of Drosophila. *J Neurosci* **28**, 13742-13753 (2008).
- 1177 74. Han, C., Jan, L.Y. & Jan, Y.N. Enhancer-driven membrane markers for analysis of
1178 nonautonomous mechanisms reveal neuron-glia interactions in Drosophila. *Proc Natl*
1179 *Acad Sci U S A* **108**, 9673-9678 (2011).
- 1180 75. Grueber, W.B., Jan, L.Y. & Jan, Y.N. Different levels of the homeodomain protein cut
1181 regulate distinct dendrite branching patterns of Drosophila multidendritic neurons. *Cell*
1182 **112**, 805-818 (2003).
- 1183 76. Kim, S.E., Coste, B., Chadha, A., Cook, B. & Patapoutian, A. The role of Drosophila
1184 Piezo in mechanical nociception. *Nature* **483**, 209-212 (2012).
- 1185 77. Petersen, L.K. & Stowers, R.S. A Gateway MultiSite recombination cloning toolkit.
1186 *PLoS One* **6**, e24531 (2011).
- 1187 78. Potter, C.J., Tasic, B., Russler, E.V., Liang, L. & Luo, L. The Q system: a repressible
1188 binary system for transgene expression, lineage tracing, and mosaic analysis. *Cell* **141**,
1189 536-548 (2010).
- 1190 79. Yakubovich, N., Silva, E.A. & O'Farrell, P.H. Nitric oxide synthase is not essential for
1191 Drosophila development. *Curr Biol* **20**, R141-142 (2010).
- 1192 80. Lacin, H. *et al.* Genome-wide identification of Drosophila Hb9 targets reveals a pivotal
1193 role in directing the transcriptome within eight neuronal lineages, including activation of
1194 nitric oxide synthase and Fd59a/Fox-D. *Dev Biol* **388**, 117-133 (2014).
- 1195 81. Ruzankina, Y. *et al.* Deletion of the developmentally essential gene ATR in adult mice
1196 leads to age-related phenotypes and stem cell loss. *Cell Stem Cell* **1**, 113-126 (2007).

- 1197 82. Lau, J. *et al.* Temporal control of gene deletion in sensory ganglia using a tamoxifen-
1198 inducible Advillin-Cre-ERT2 recombinase mouse. *Mol Pain* **7**, 100 (2011).
- 1199 83. Cahalan, S.M. *et al.* Piezo1 links mechanical forces to red blood cell volume. *Elife* **4**
1200 (2015).
- 1201 84. Stone, M.C., Albertson, R.M., Chen, L. & Rolls, M.M. Dendrite injury triggers DLK-
1202 independent regeneration. *Cell reports* **6**, 247-253 (2014).
- 1203 85. Emoto, K., Parrish, J.Z., Jan, L.Y. & Jan, Y.N. The tumour suppressor Hippo acts with
1204 the NDR kinases in dendritic tiling and maintenance. *Nature* **443**, 210-213 (2006).
- 1205 86. Parrish, J.Z., Emoto, K., Kim, M.D. & Jan, Y.N. Mechanisms that regulate establishment,
1206 maintenance, and remodeling of dendritic fields. *Annu Rev Neurosci* **30**, 399-423 (2007).
- 1207 87. Park, J.W., Vahidi, B., Taylor, A.M., Rhee, S.W. & Jeon, N.L. Microfluidic culture
1208 platform for neuroscience research. *Nature protocols* **1**, 2128-2136 (2006).
- 1209 88. Weng, Y.L. *et al.* An Intrinsic Epigenetic Barrier for Functional Axon Regeneration.
1210 *Neuron* **94**, 337-346 e336 (2017).
- 1211 89. Pogoda, K. *et al.* Soft Substrates Containing Hyaluronan Mimic the Effects of Increased
1212 Stiffness on Morphology, Motility, and Proliferation of Glioma Cells.
1213 *Biomacromolecules* **18**, 3040-3051 (2017).
- 1214 90. Longair, M.H., Baker, D.A. & Armstrong, J.D. Simple Neurite Tracer: open source
1215 software for reconstruction, visualization and analysis of neuronal processes.
1216 *Bioinformatics* **27**, 2453-2454 (2011).

Figure 1

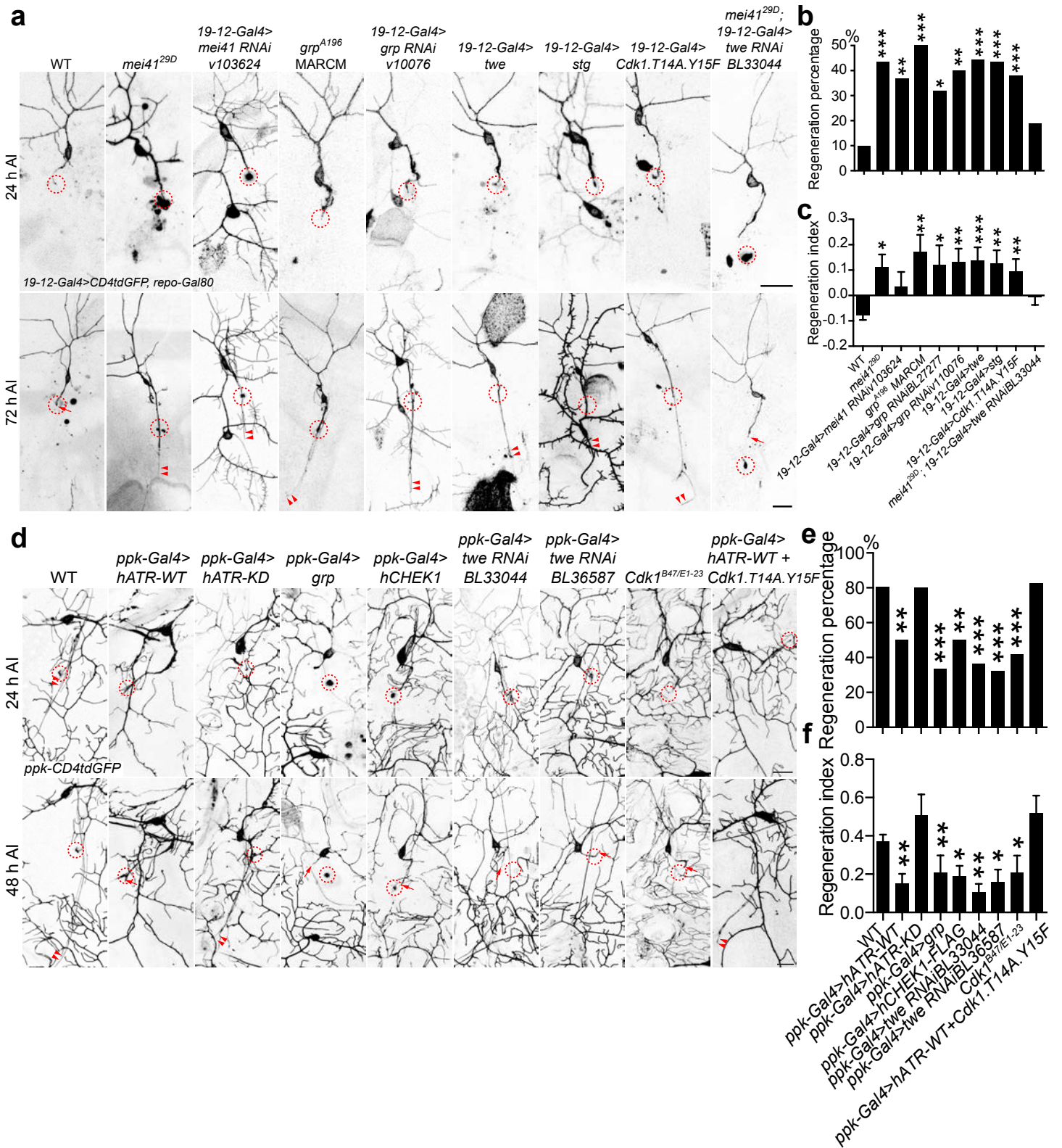


Figure 2

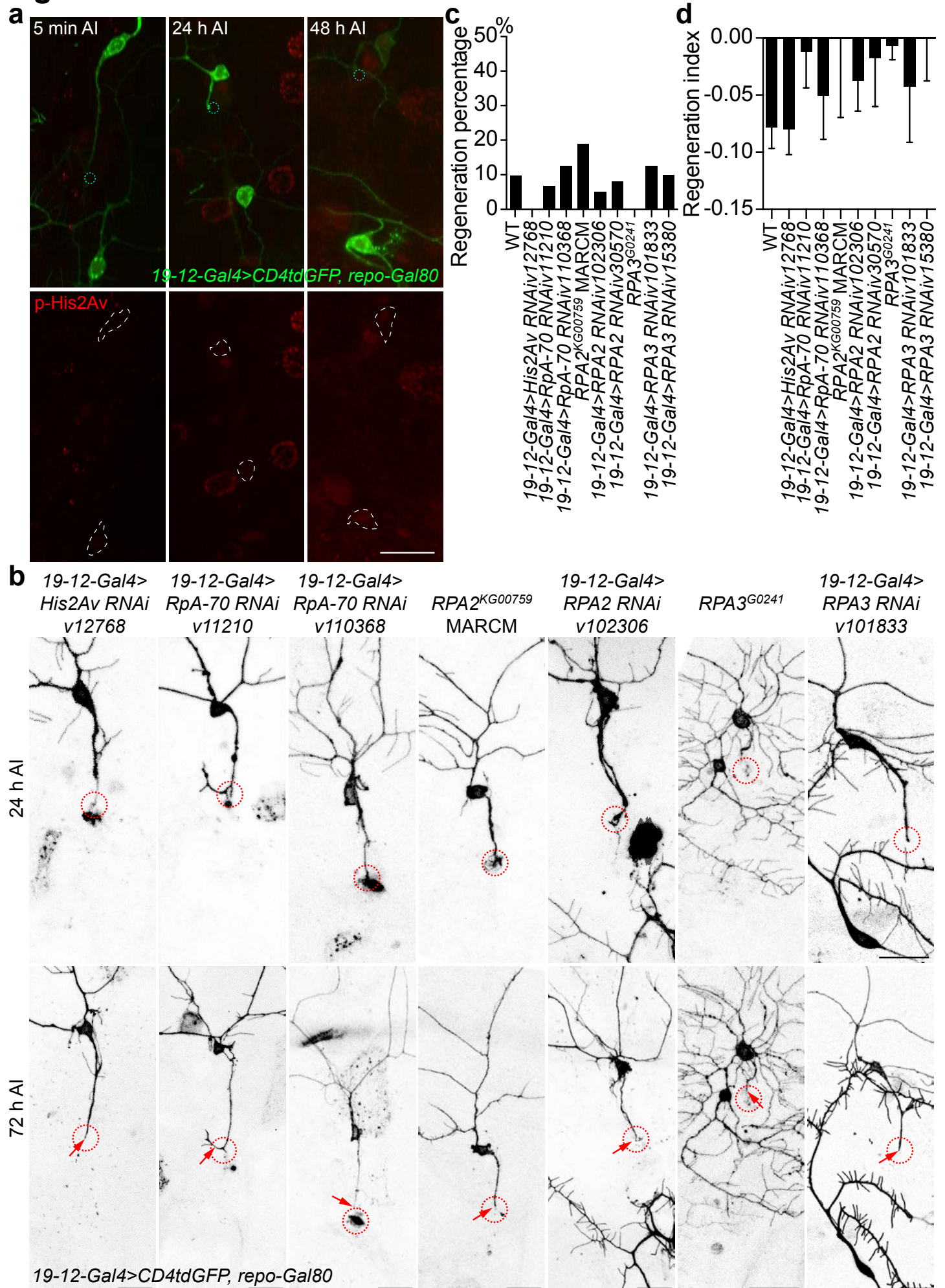


Figure 3

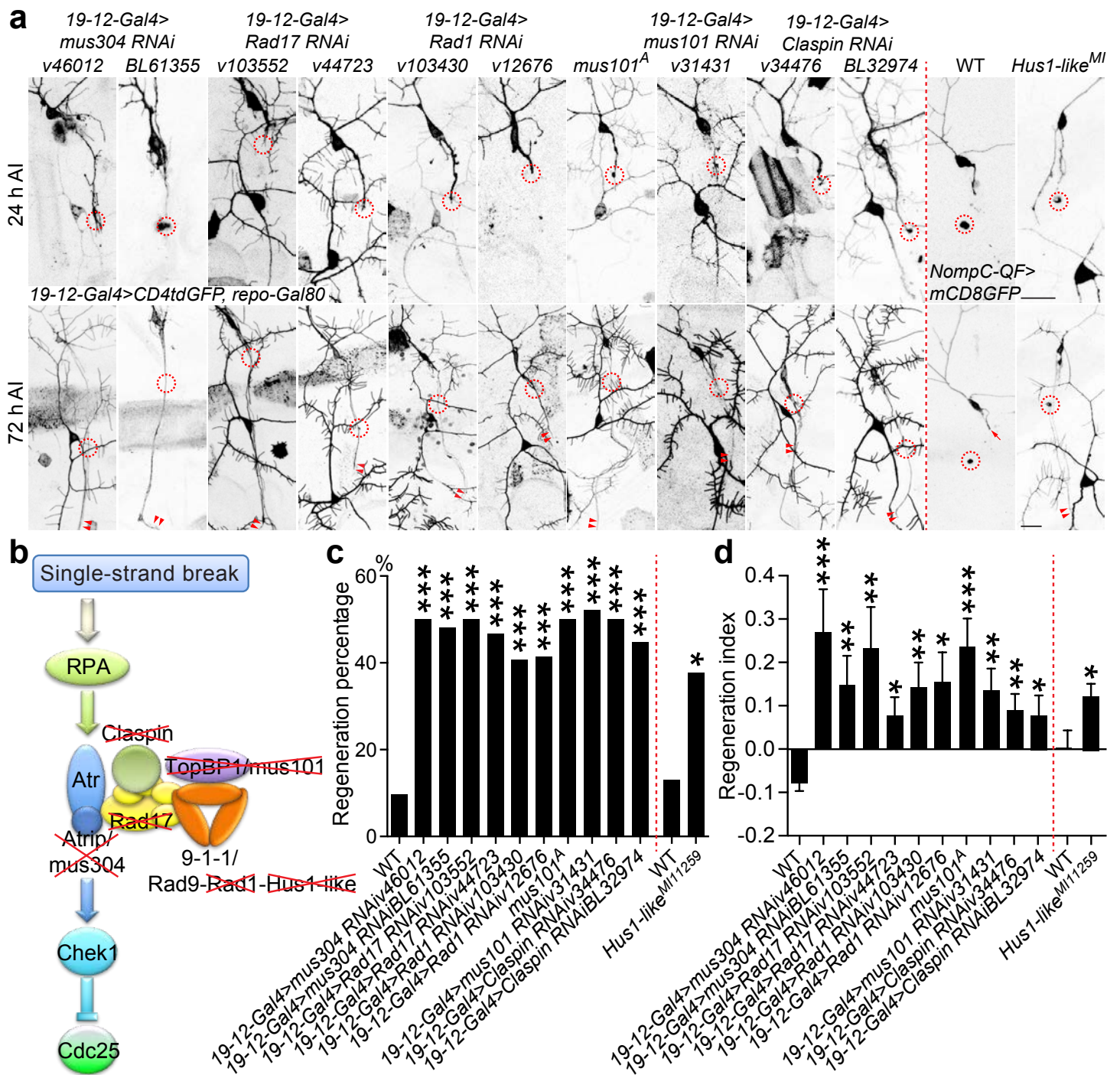


Figure 4

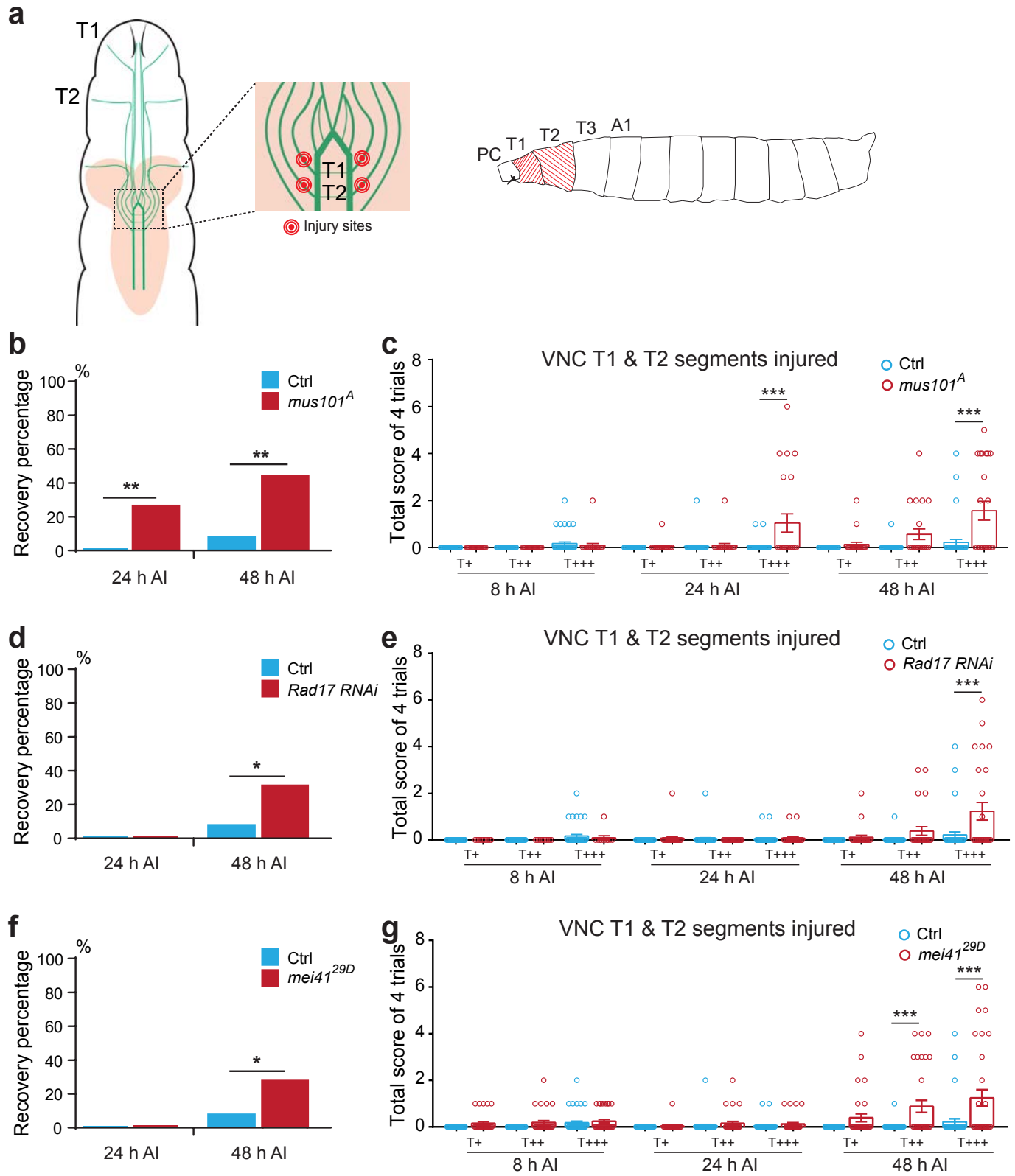


Figure 5

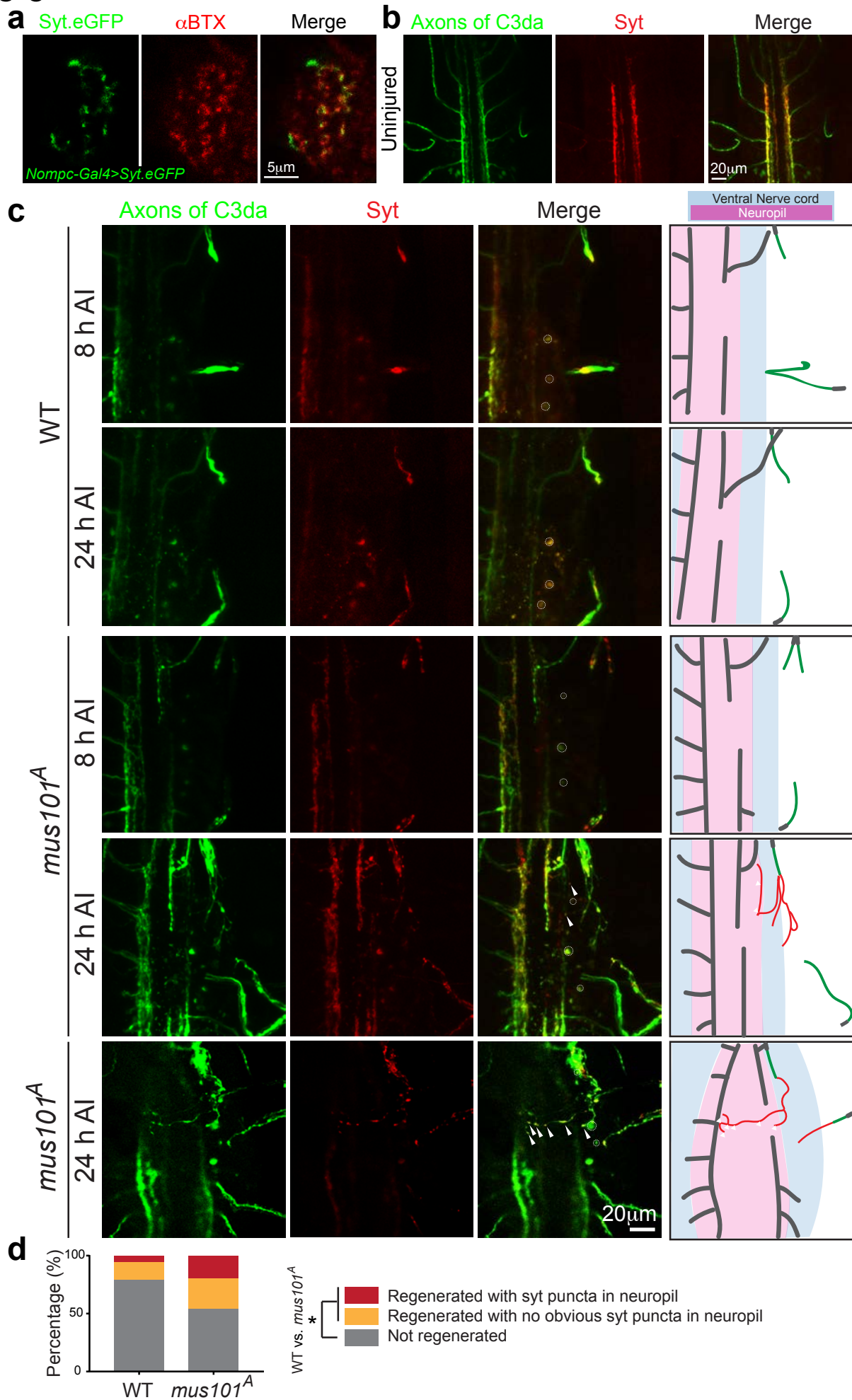


Figure 6

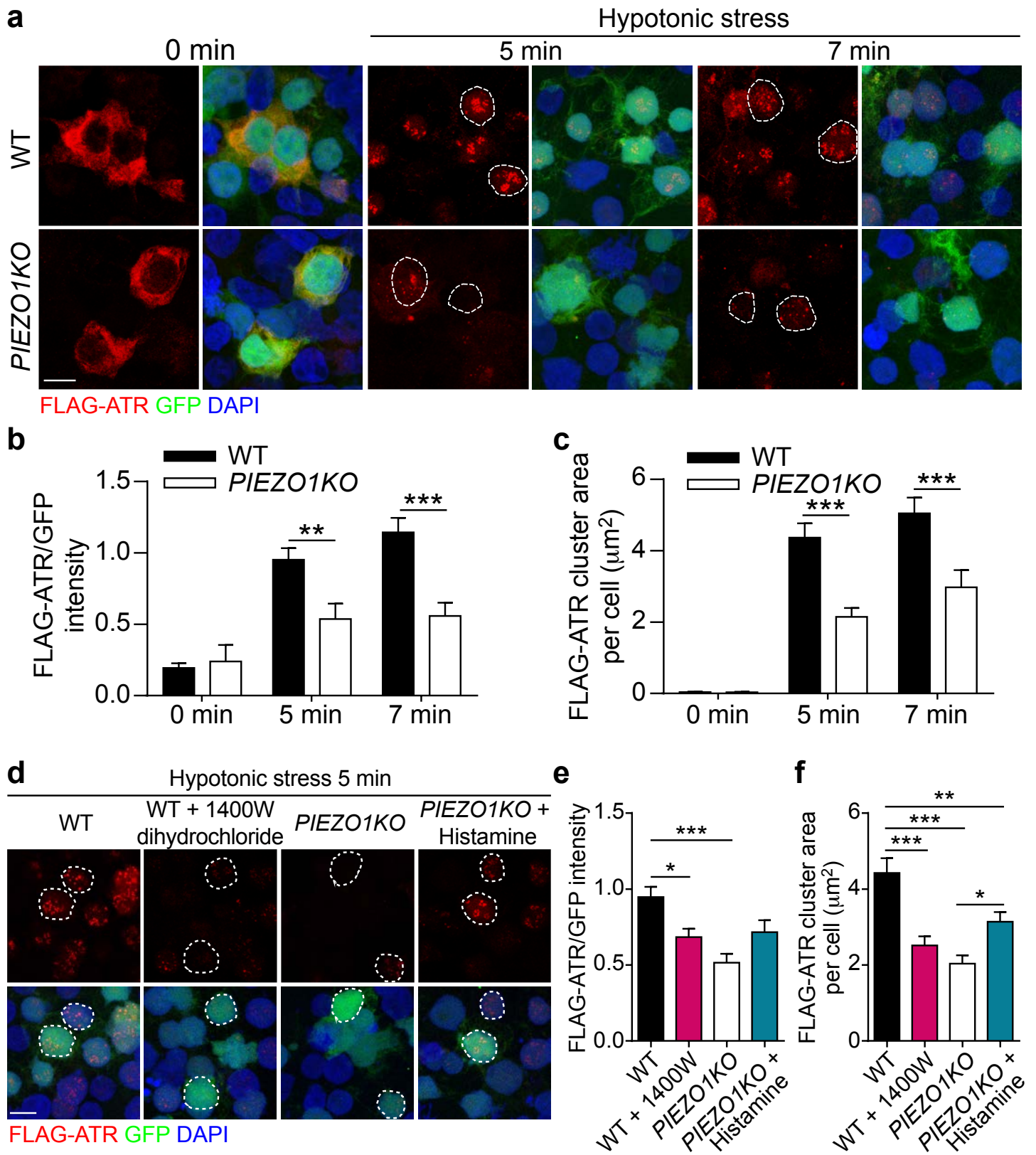


Figure 7

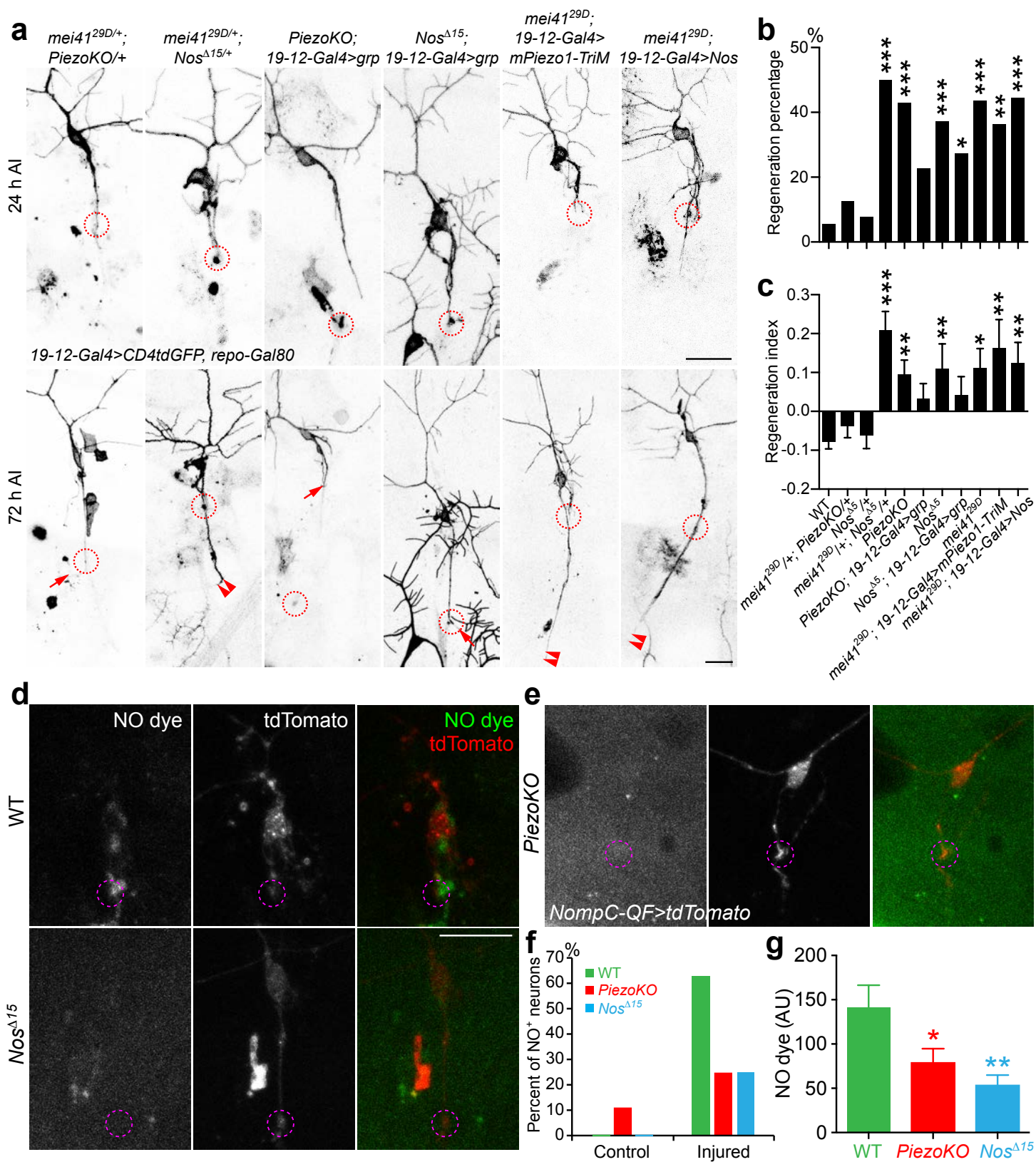
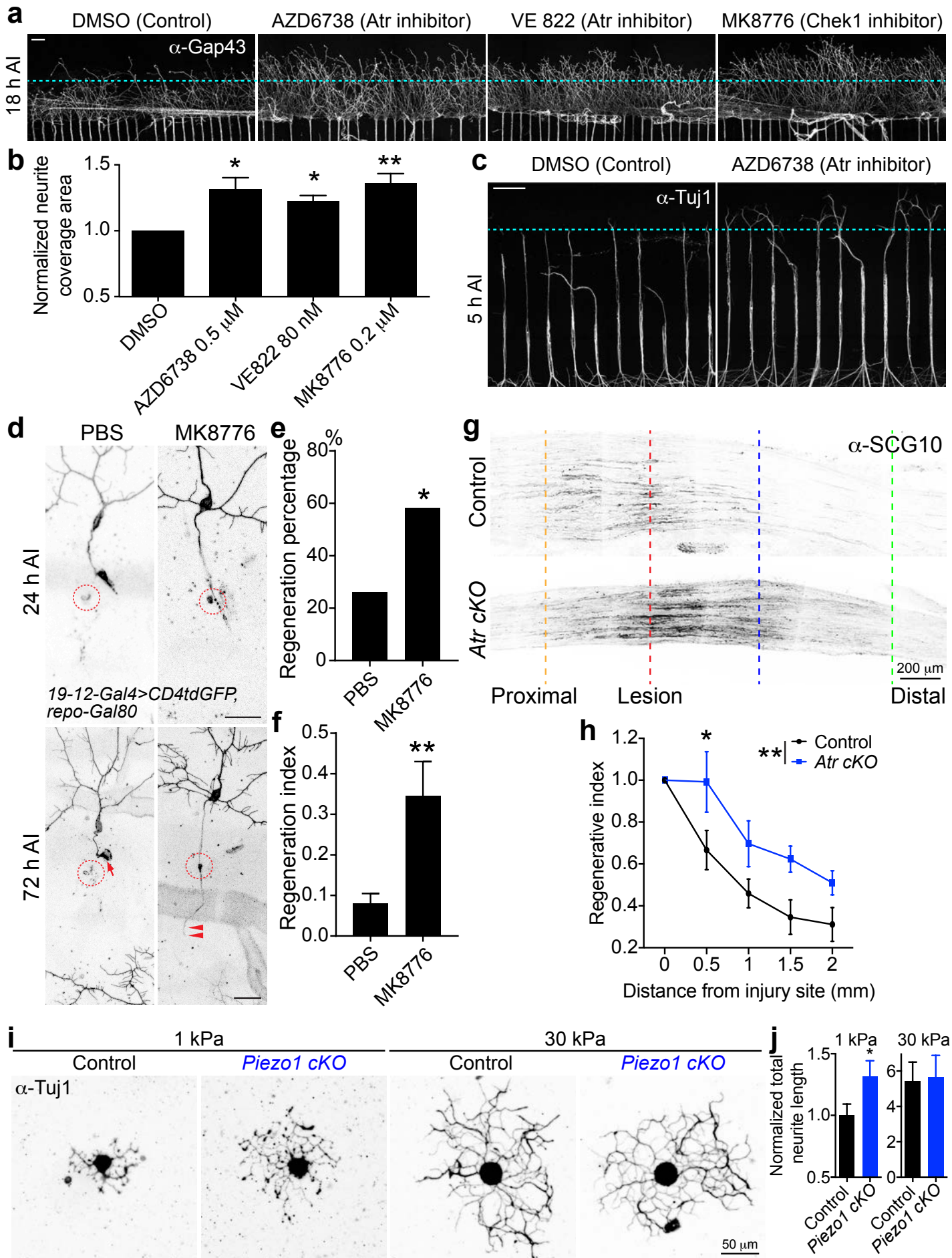
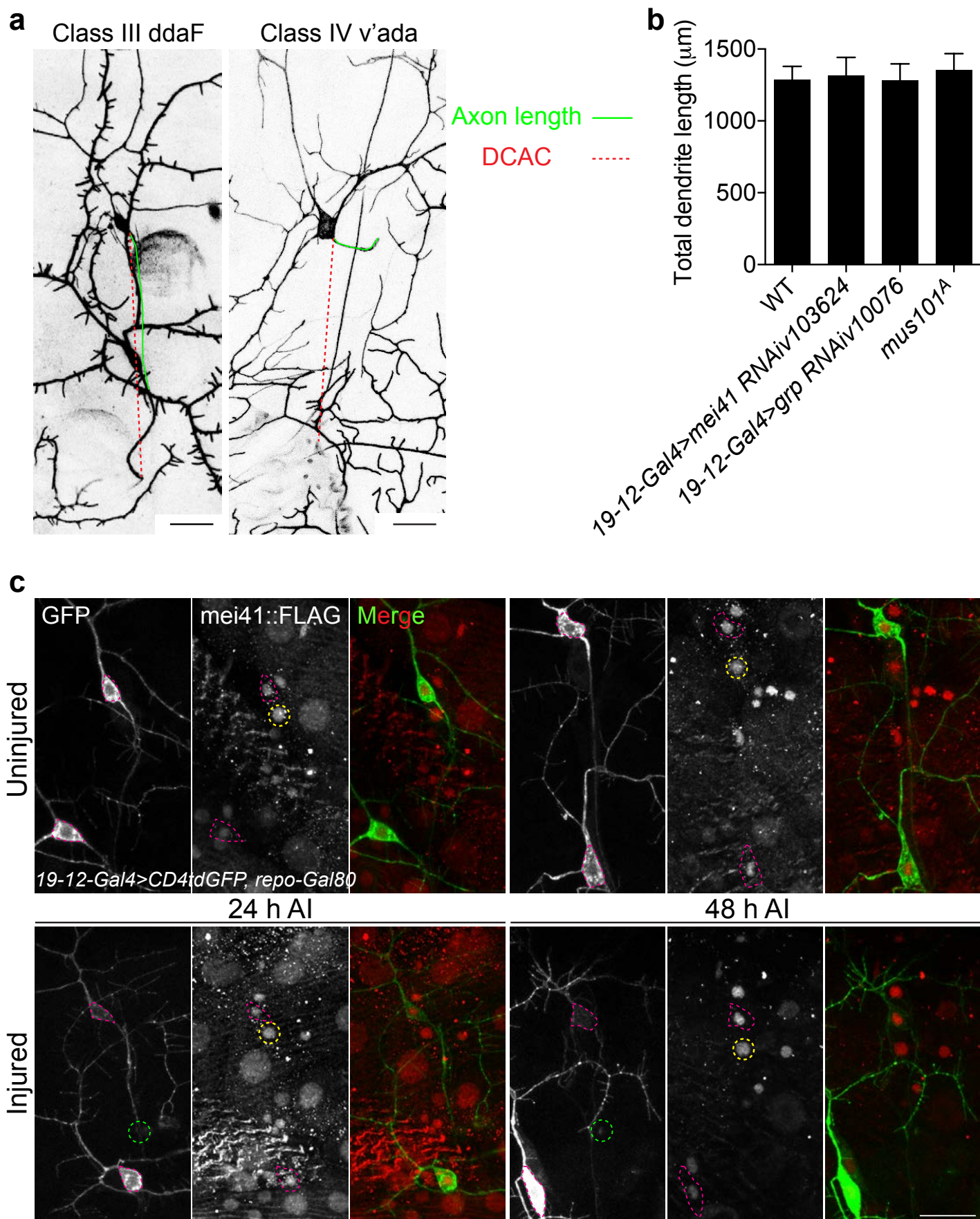


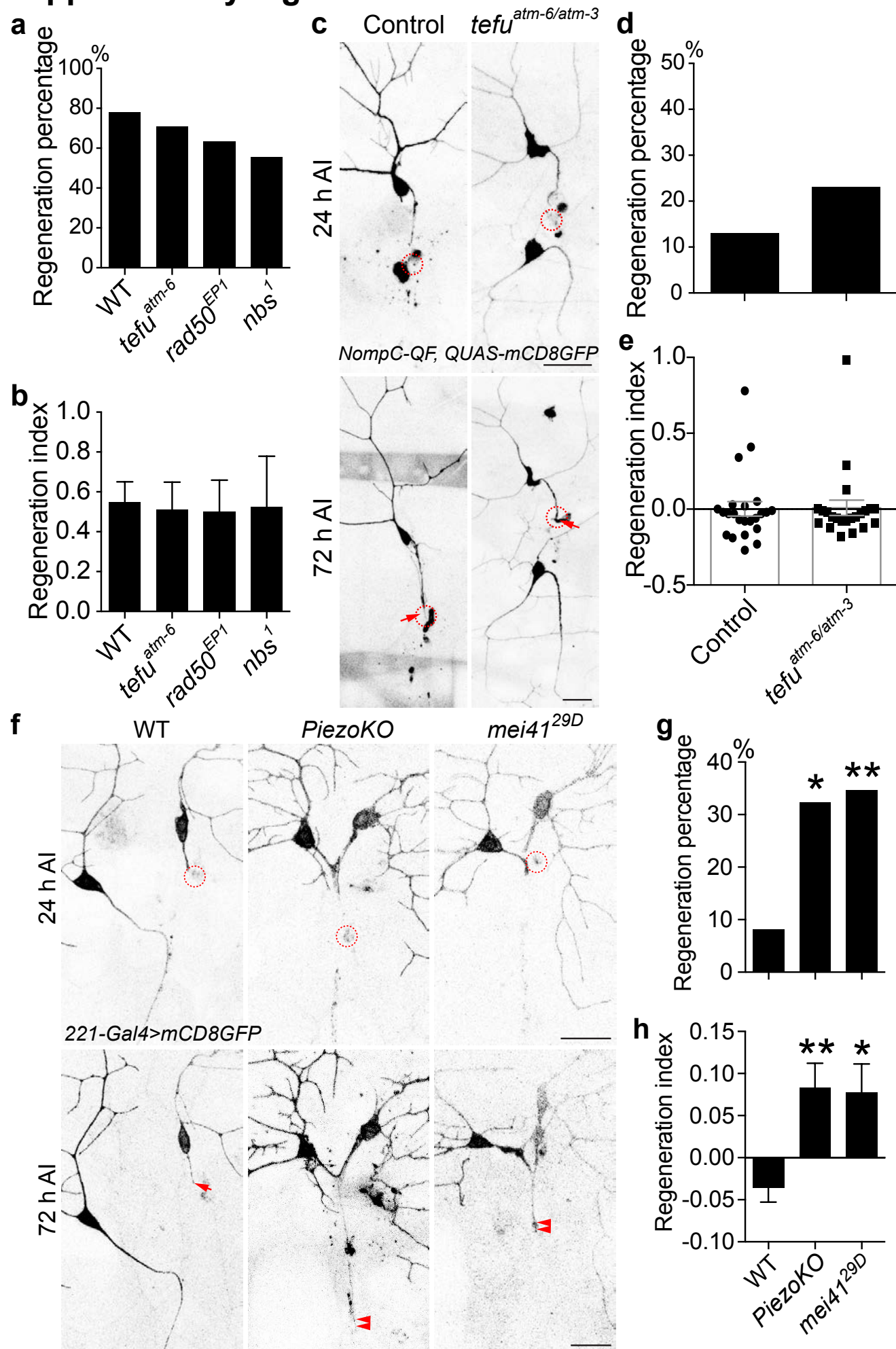
Figure 8



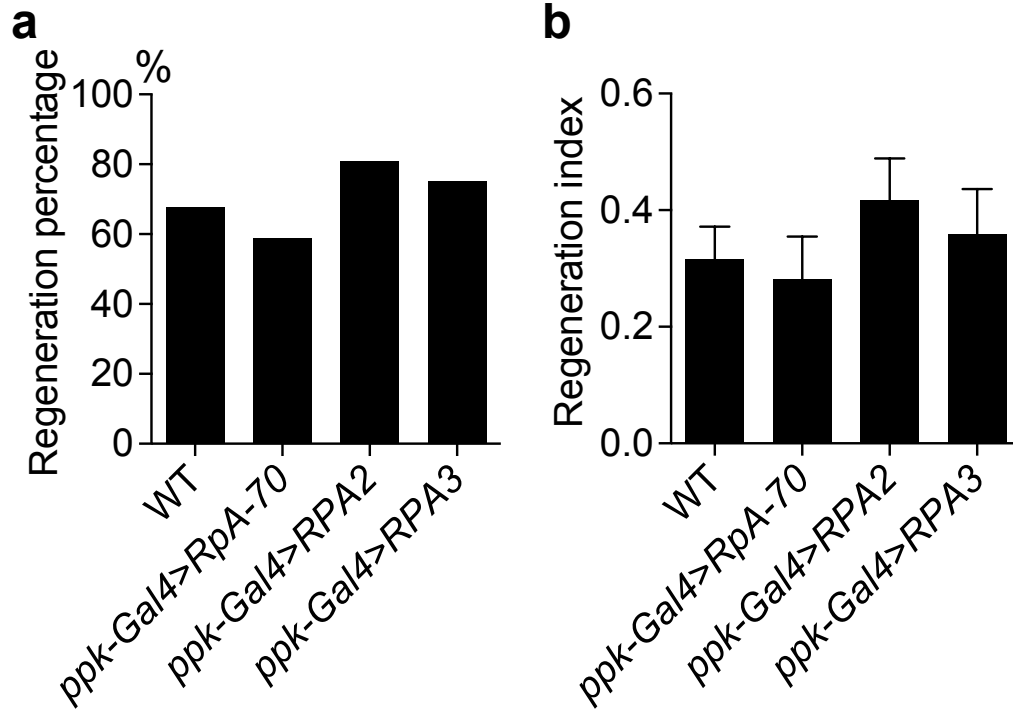
Supplementary Figure 1



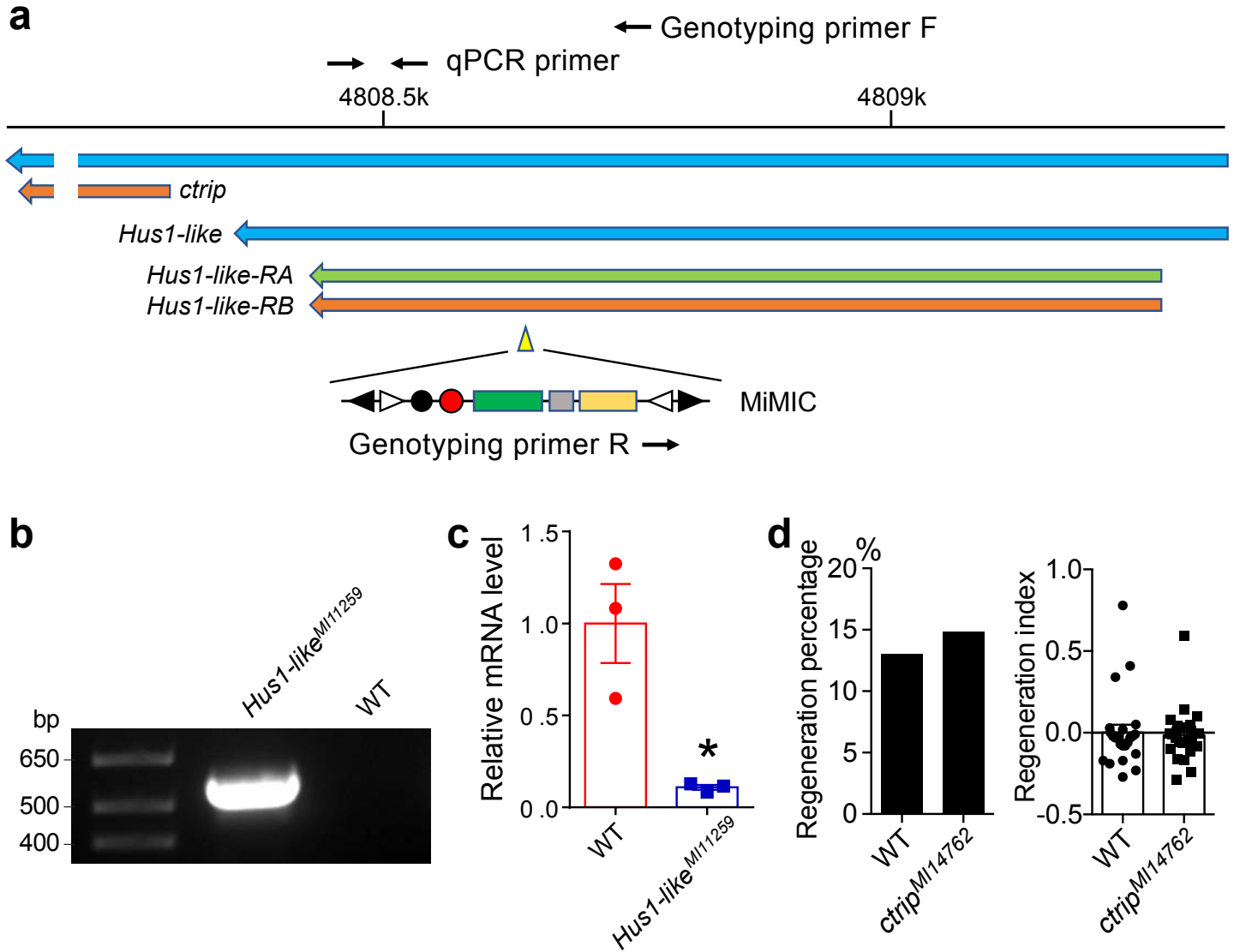
Supplementary Figure 2



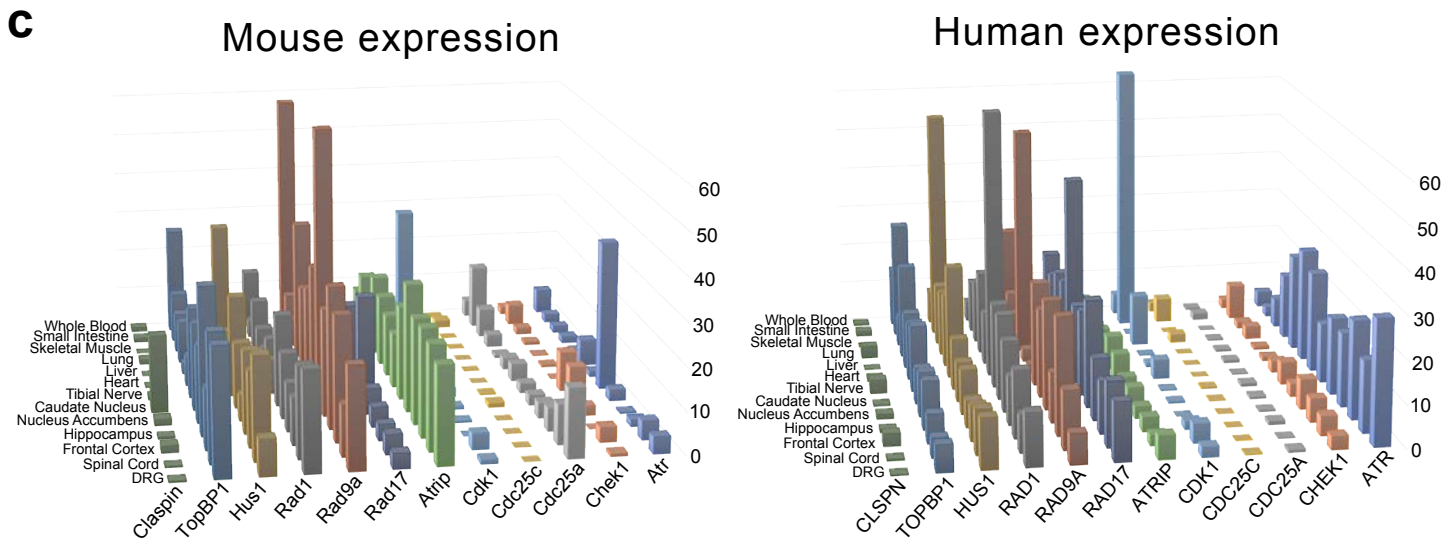
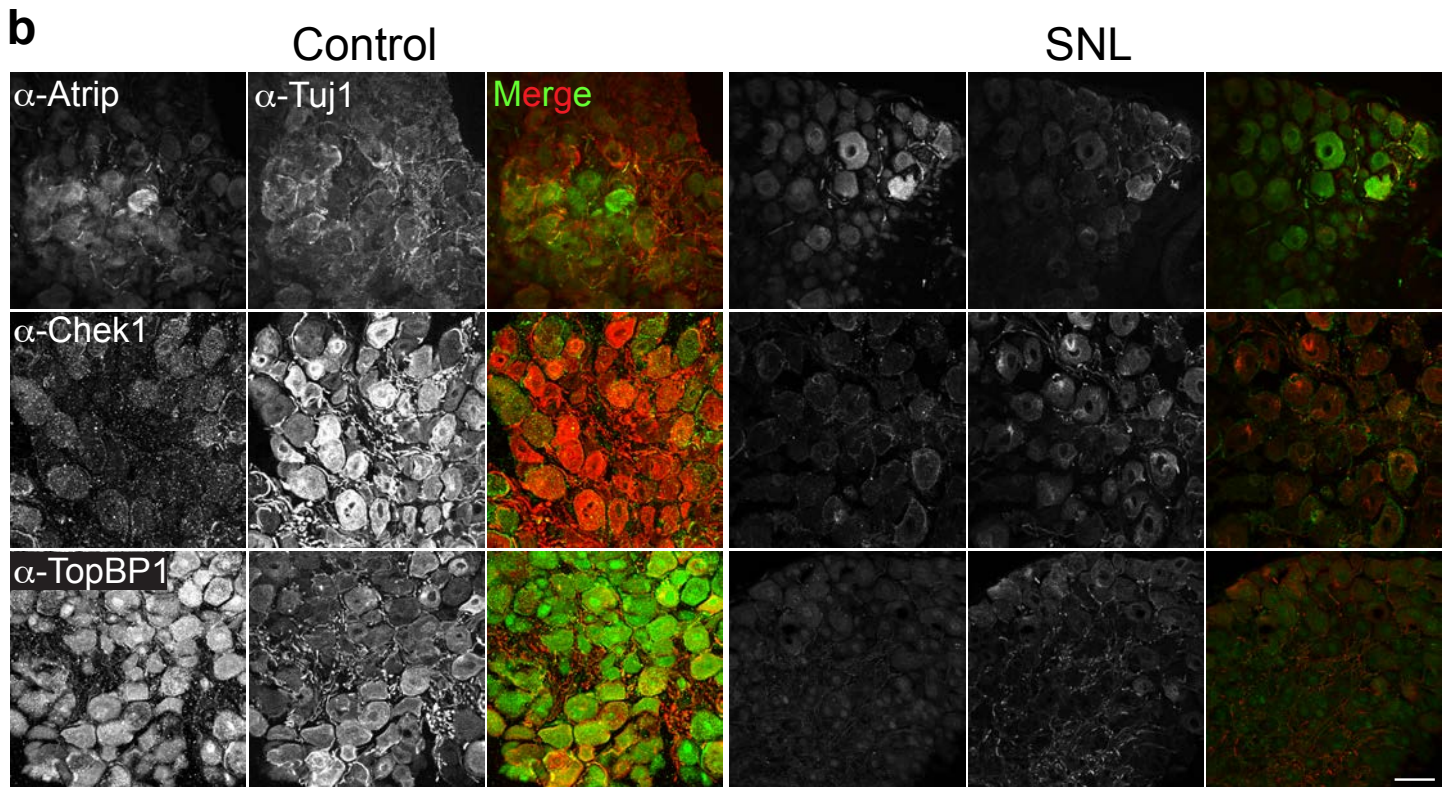
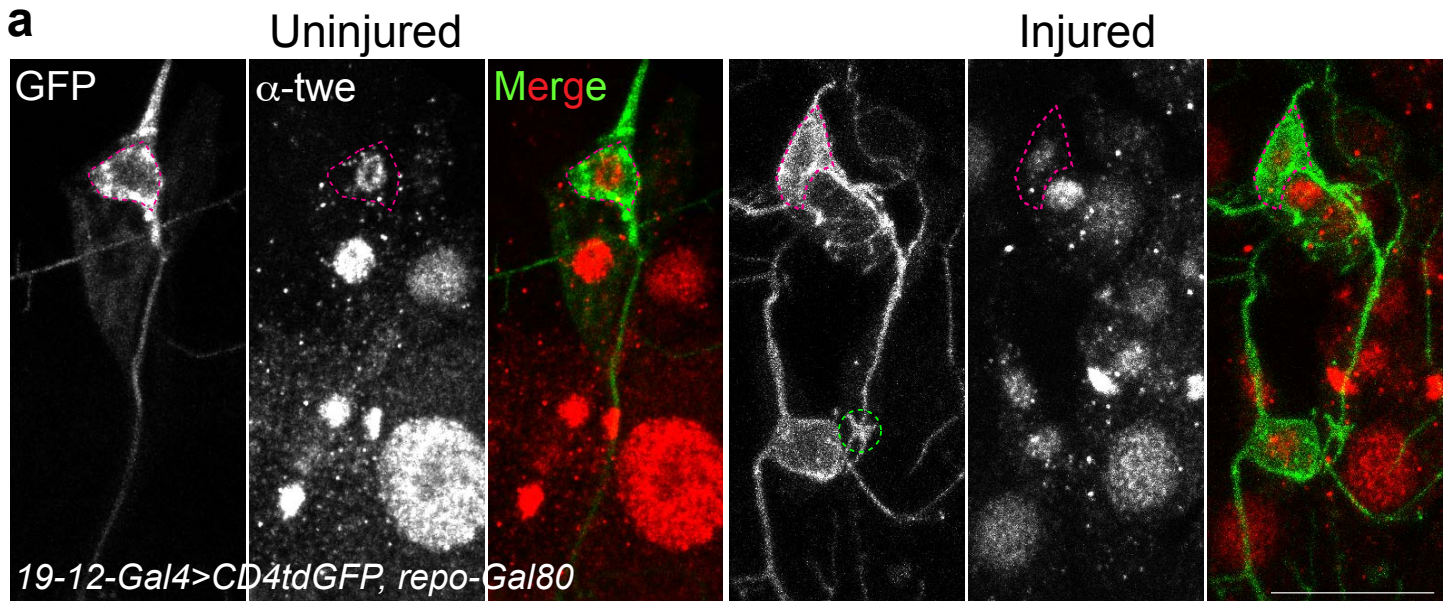
Supplementary Figure 3



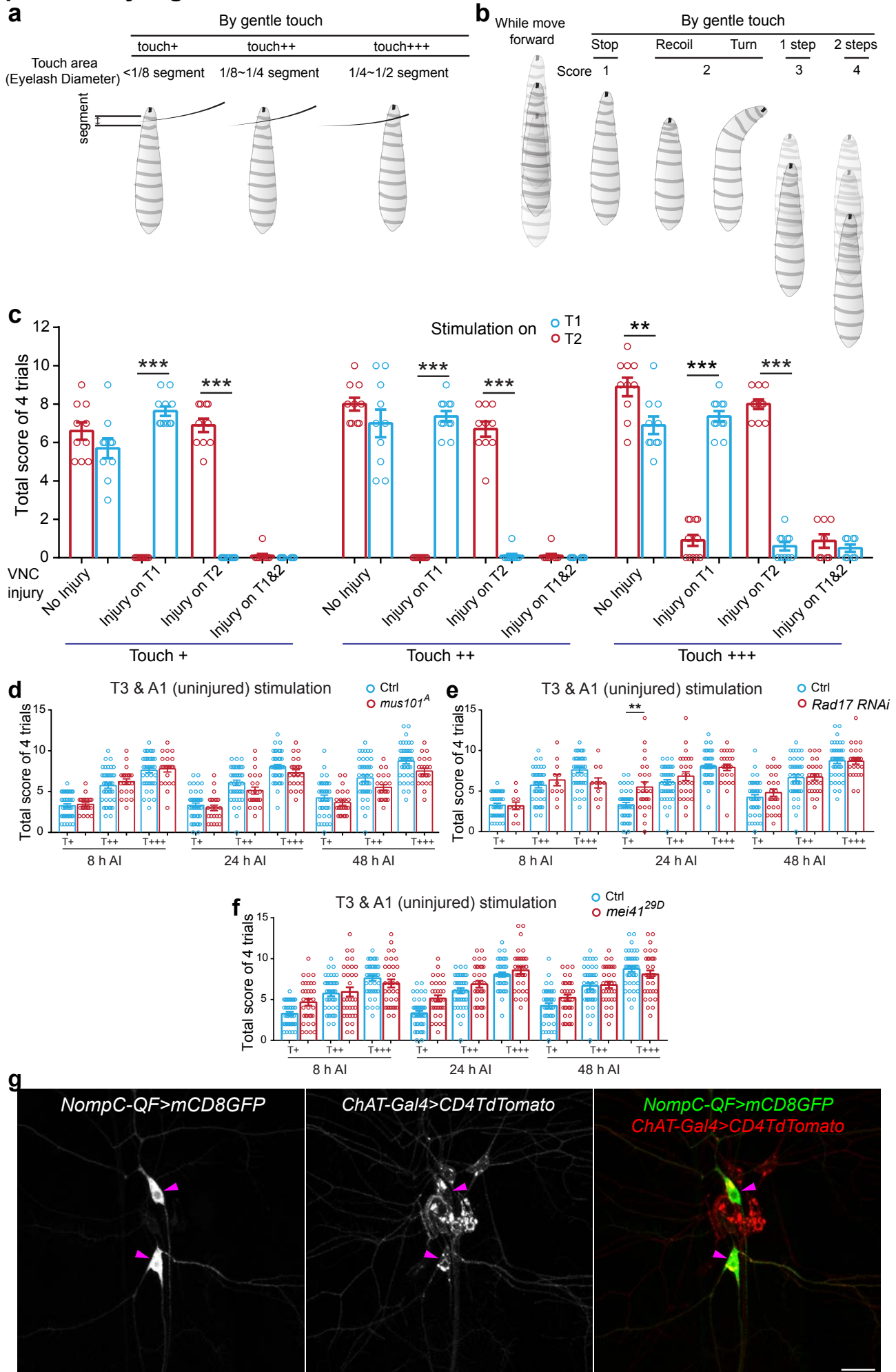
Supplementary Figure 4



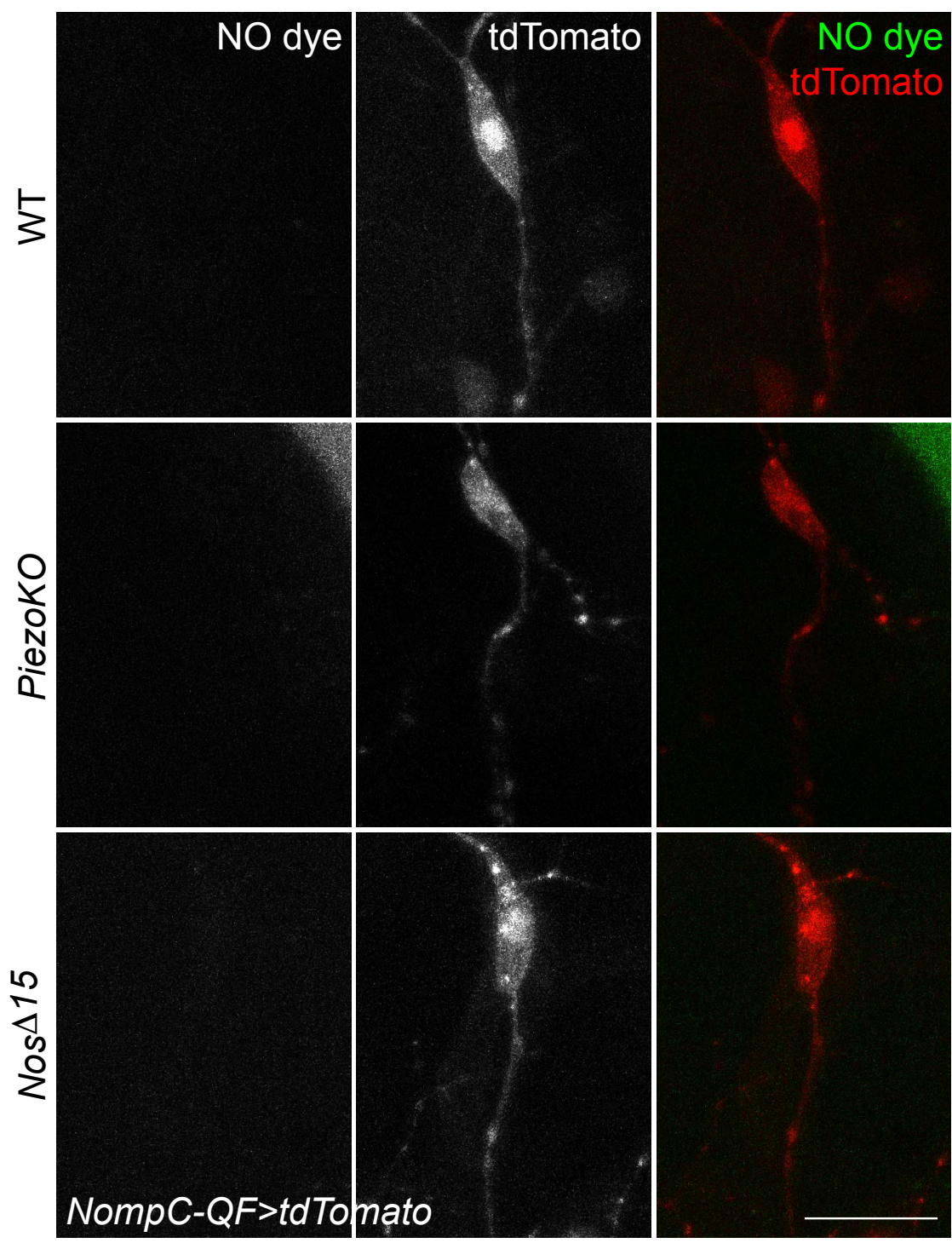
Supplementary Figure 5



Supplementary Figure 6



Supplementary Figure 7



Supplementary Figure 8

